PET Molecular Imaging & Its Biological Applications
M.E. Phelps, ed. Springer, NY, 2003

# The Molecular Basis of Disease

*Jorge R. Barrio*

For as long as man has lived, he has been concerned with health and well being. Much of human history has revolved around uncontrollable diseases; many critical events, wars, and even the fate of many societies have been determined by human health. Medicine is as old as human history and has evolved from mystical and religious beginnings to the scientific discipline of today.

The boundaries of medical knowledge are continually expanding. A modern definition of disease as: *a disordered or incorrectly functioning organ, part structure, or system of the body resulting from the effect of genetic or developmental errors, infection, poisons, nutritional deficiency or imbalance, toxicity, or unfavorable environmental factors*[1] hints at the chemical basis of disease. We can further say that disease results from a disruption of the chemical homeostasis of the body or, in other words, a disruption of a tendency to dynamic stability in the normal body states of the organism. Alteration of chemical homeostasis can be induced by internal or external factors resulting in specific biochemical abnormalities that change normal organ function to the point that clinical symptoms are produced. Today, however, the technical elements of medical practice to diagnose and treat disease still are—for the most part—anatomical in nature. Practicing physicians order—and feel comfortable with—computerized tomography (CT), magnetic resonance imaging (MRI) scans, and ultrasound but have been slow to incorporate biological criteria from molecular imaging techniques such as positron emission tomography (PET) into their practice.

In classical medical practice, biological abnormalities are typically tested clinically and by determining biochemical parameters at a distance from the involved organ. Kidney function, for example, is assessed by measuring creatinine, phosphate, and urea plasma levels; liver function is similarly assessed with specific liver markers (e.g., transaminases) also in plasma. Moreover, from ancient times, physicians have ordered prescriptions for their patients that are attempts at restoring a disturbed chemical imbalance of disease. Drugs are used to reverse or control chemical imbalances by targeting key enzymes, transporters, and receptor systems. In sufficient amounts, drugs are used to either block or inhibit specific pathways in neurotransmission (e.g., neuroleptics binding to dopamine-

D2 receptors to control schizophrenic symptoms), supplement substrates when enzyme deficits exist [e.g., L-DOPA to treat Parkinson's disease where central dopaminergic aromatic amino-acid decarboxylase (AAAD) concentration is decreased], or inhibit specific tumor enzymes with the aim of destroying tumor cells (e.g., 5-fluorouracil to inhibit thymidylate synthetase).

If living organisms are governed by chemical homeostasis, some conclusions can be established:

1. Chemical disturbances will precede anatomical abnormalities in disease. It is now well established, for example, that genetic mutations or loss of regulated expression of genes will precede clinical symptoms of cancer by many years, perhaps decades. Similarly, Parkinson's disease and Alzheimer's disease have subclinical stages for years wherein the brain can control degenerative processes by adjusting function through compensating mechanisms of neuronal plasticity or through biochemical reserves controlling neuronal processes.
2. As a result of (1), above, diagnostic procedures using imaging probes aimed at detecting these biochemical abnormalities will permit earlier and informative detection of disease, sometimes many years ahead of conventional medical practice. This concept was demonstrated in Huntington's disease, a familial neurodegenerative disease that could be detected with PET studies of glucose metabolism seven years before symptoms develop.[2] More recently, preclinical assessment of Alzheimer's disease was also made possible using similar PET metabolic studies in patients with increased predisposition for the disease due to their carrying the APOE4 gene.[3]
3. Imaging probes (diagnostic) and drugs (therapeutics) share common concepts in structural design and principle of action because they target the same enzymes, receptors, and neurotransmitter systems. Drugs, through mass action, block or inhibit their targets and, thus, restore chemical imbalances conducive to control or diminish or remove clinical symptoms. Molecular imaging probes, at tracer levels, probe the same targets assessing their functional status. Thus, drugs and molecular imaging probes typically share structural requirements, being the same molecule or structural analogs of each other (Figure 4-1).

When using molecular imaging probes, it is always necessary to consider that the ultimate objective of a PET determination is quantitation of the process that is measured. Tracer kinetic techniques are generally used to monitor dynamic processes with PET, namely tissue perfusion, local metabolic processes (e.g., glucose metabolic rates in the brain, the heart, and tumors), synthesis processes (e.g., protein and neurotransmitter synthesis), receptor properties (e.g., their number and affinities), and so on (Chapter 2). Accurate estimation of quantitative parameters requires formulation of a tracer kinetic model according to the process to be measured and the biochemical or pharmacologic information available at the time.

Steps to develop a successful tracer kinetic model are:

1. Molecular probe design and synthesis.
2. Formulation of a workable model.
3. Model validation.
4. Model application.

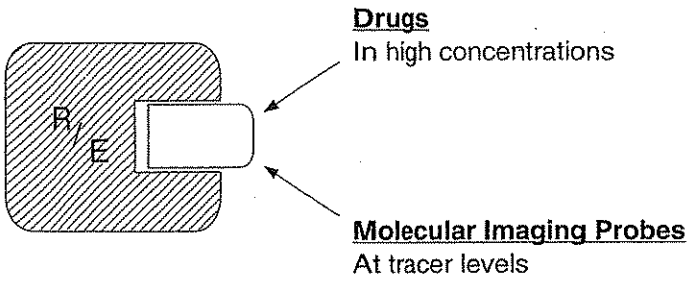


FIGURE 4-1. Schematic diagram indicating common targets [e.g., enzyme (E) or receptor proteins (R)] for drugs and molecular imaging probes.

The process is iterative to achieve maximum accuracy and success. When the process is understood and demonstrated to be generally effective, other quantitative (or semiquantitative) approaches are developed to simplify the utilization of the procedure. Ultimately, the molecular imaging probe is introduced in the clinic for routine use. The best example of a positron-emitting molecular imaging probe going through this evolutionary pathway is 2-deoxy-2-[F-18]fluoro-deoxy-D-glucose (FDG). Other pharmaceuticals have also followed this pathway and are now entering the clinical arena, like [N-13] ammonia as a myocardial perfusion agent and 6-[F-18]fluoro-L-DOPA as a probe of central dopaminergic system integrity. Many other PET probes have been developed and thoroughly studied but have not yet become available for routine clinical use. This chapter will focus on molecular probe design to develop an understanding of the noninvasive biochemical or pharmacological process to be measured with PET. For all other mathematical aspects of tracer kinetic modeling, the reader is referred to Chapter 2 and other excellent publications in the field.[4]

## MOLECULAR PROBE DESIGN: GENERAL PRINCIPLES

In order to obtain meaningful results, investigations of living organisms must be performed with a minimum of interference with the system under investigation. The introduction of radioactive molecules into the system is one of the preferred alternatives for the study of biological systems because it produces only minimal experimental disturbances, due to the extremely low mass of the probe, and thus allows one to distinguish the experimental components from the background (Figure 4-2). Most of the present knowledge of biochemistry, particularly metabolism, has been obtained by the use of radioactive (carbon-14 and tritium) and stable (deuterium, carbon-13, and nitrogen-15) isotopes. For a variety of reasons, however, these isotopes are not adequate for the noninvasive assessment of physiological and biochemical processes. Even though tracer techniques have led to the development of useful clinical applications (e.g., conventional nuclear medicine techniques), the development of PET has led the way in the development and use of quantitative assays of local biochemical and pharmacological processes in humans.

### Properties of molecular imaging probes labeled with positron-emitting radioisotopes

Some important properties that make molecular imaging probes used with PET very valuable for the *in-vivo* assessment of biochemical and pharmacological processes in humans can be summarized as follows:

1. Compounds labeled with positron-emitting radioisotopes can be prepared with high-specific activity (Chapter 3) so that the process to be measured is not perturbed.
2. Gamma rays produced after positron annihilation allow for quantitative high resolution imaging (Chapter 1).
3. With cyclotron-produced positron-emitting radioisotopes of carbon (C-11; t 1/2 = 20.38 min), nitrogen (N-13; t 1/2 = 9.96 min), oxygen (O-15; t 1/2 = 2.03 min) and fluorine (F-18; t1/2 = 109.72 min) (Chapter 3), true molecular imaging probes matching the strict requirements of enzyme and/or receptor targets can be designed. The design of these molecular probes takes advantage of the following: (a) labeling with the most common positron-emitting radioisotopes, carbon-11, nitrogen-13, and oxygen-15, renders compounds biochemically indistinguishable from their natural counterparts; and (b) fluorine-18 can be used to provide labeled substrate analogs (e.g., FDG) or pharmacological agents (F-18-labeled spiperone) to trace biochemical or pharmacological processes in a predictable manner. Fluorine is an important element used to modify biologically active compounds (e.g., in drug design). Because of its small size and the strength of the C-F bond, fluorine is commonly used to replace H or OH on a molecule. This modification allows favorable interactions of the new molecule (e.g., molecular imaging probe, drug) with the target (e.g., enzyme, receptor) to occur without steric hindrance. Moreover, the presence of fluorine may block, with target enzymes, subsequent reactions in a given pathway.
4. The positron emitters carbon-11, nitrogen-13, oxygen-15, and fluorine-18 constitute the only externally detectable forms of carbon, nitrogen, oxygen,

**FIGURE 4-2.** Molecular imaging probes as reporters in *in-vivo* systems.

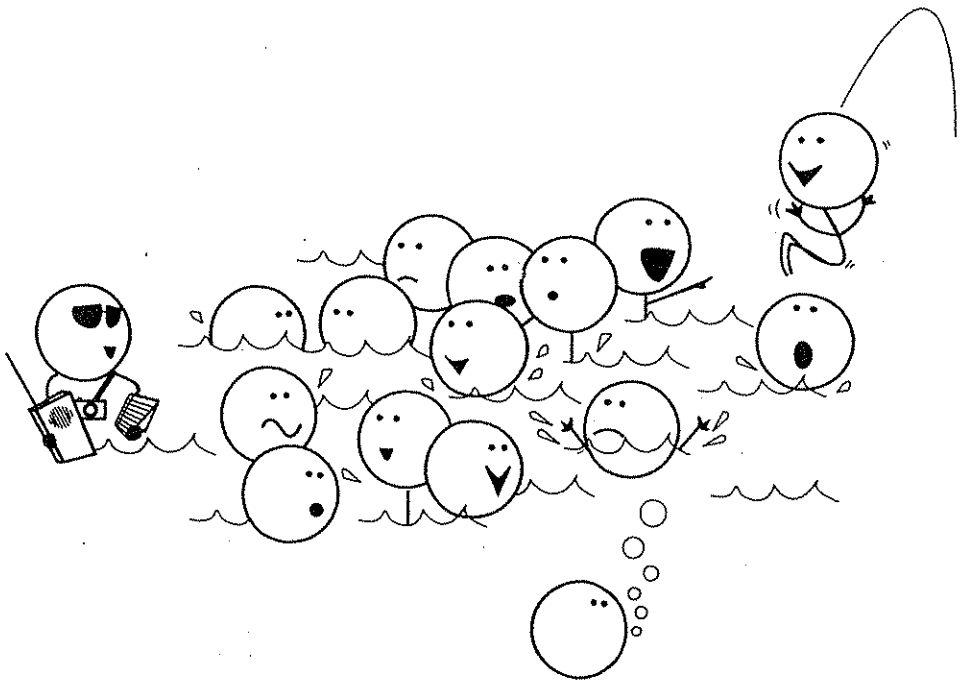

and fluorine, respectively. The time course of radioactive emission can be readily quantitated with PET, permitting the application of tracer kinetic techniques for the measurement of substrate concentrations, reaction rates, and receptor binding in tissue.
5. The short half-lives of these isotopes permit extension of these determinations to humans.

### General criteria for selecting and using molecular imaging probes

The question of whether a specific compound can be labeled with a positron emitter, with the intention of using that probe as a molecular imaging agent, is often asked. There is, however, much more to the effective design of molecular imaging probes than this question alone. Indeed, it is the wrong question altogether if it is not preceded by a complete understanding of the structural requirements of the target enzyme or receptor and the process to be measured. To select a molecular imaging probe to measure a specific process or assess organ function, the probe should meet the following criteria:

1. Target specificity—ideally, the probe should be restricted to the target process.
2. High membrane permeability to reach target areas.
3. As a result of a specific interaction with a target molecule in tissue, trapping of the labeled molecule or labeled reaction product should occur in a slow turnover pool.
4. Use of analogs specific to one biochemical pathway to isolate one step or a few steps of the process—thus, the kinetics of only the administered compound is represented in the measured data.
5. Rapid turnover rates (small precursor pool) for the substrate precursor are desirable to allow reaction of the labeled molecule probe to proceed rapidly and, thus, reduce background signal rapidly. This implies high affinity of the molecular probe for its tissue target and rapid clearance of the probe from nonspecific areas.
6. Rapid blood pool clearance of the molecular imaging probe to reduce blood pool background at the tissue target (e.g., brain, heart, and tumor) and increase the rate of clearance of the probe from tissue as a result of the temporal decrease in probe concentration in blood.
7. No—or—slow peripheral metabolism of the probe to have the administered probe as the only—or—primary chemical entity in blood.
8. High-specific activity (low masses at the radioactivity concentrations used; Chapter 3) to trace the process under investigation without exerting mass effects on the target molecule.
9. Low nonspecific binding to increase target specificity and target-to-background ratios $>> 1$.
10. A small number of transport and biochemical reaction steps for the molecular imaging probe to allow tracer kinetic modeling to establish quantitative parameters for the imaging determination (Chapter 2).

## TYPES OF MOLECULAR IMAGING PROBES

As indicated earlier, to assess biochemical disturbances (e.g., disease states) noninvasively using molecular imaging with PET, specific probes are designed and used to target the process to be investigated (e.g., glucose metabolism, neuro-

transmitter synthesis, neurotransmitter re-uptake, postsynaptic receptor binding, protein synthesis, gene expression, and so on). In general, these molecular probes should have specific properties. Based on the target molecule in tissue, PET imaging probes are divided into three large groups: 1) Probes based on enzyme-mediated transformations; 2) Probes based on stoichiometric binding interactions; and 3) Probes for determination of perfusion. With a few exceptions (e.g., [N-13]ammonia), the latter probes have no specific structural requirements, except for their high vascular membrane permeability without specific macromolecular targets in tissue. The reader is referred to Chapter 2 for review of the assays for tissue perfusion determinations.

## Probes based on enzyme-mediated transformations

These probes are characterized by trapping in tissue the product of a specific interaction of the probe with an enzyme. This interaction will normally produce a chemical transformation of the original probe catalyzed by the enzyme that is being targeted. The product of the enzyme-mediated transformation (e.g., phosphorylated substrate) is impermeable to cell membranes and is, therefore, retained in tissue in proportion to the rate of reaction of the enzyme-mediated process. The process has been called metabolic trapping (Figure 4-3).

The best known examples of PET imaging probes acting through this mechanism are 1) hexokinase-mediated trapping of FDG-6-phosphate after FDG administration in the estimation of local glucose metabolic rates in tissue; 2) aromatic amino acid decarboxylase-mediated transformation of 6-[F-18]fluoro-L-DOPA (FDOPA) into 6-[F-18]fluorodopamine with subsequent storage in vesicles in central dopaminergic terminals; 3) the herpes simplex thymidylate kinase (HSV1-TK) model of gene expression that mediates trapping of radiofluorinated acycloguanosines and thymidine analogs to their corresponding 5′-phosphates; and 4) 3′-[F-18]fluoro-3′-deoxythymidine ([F-18]FLT) used in the assessment

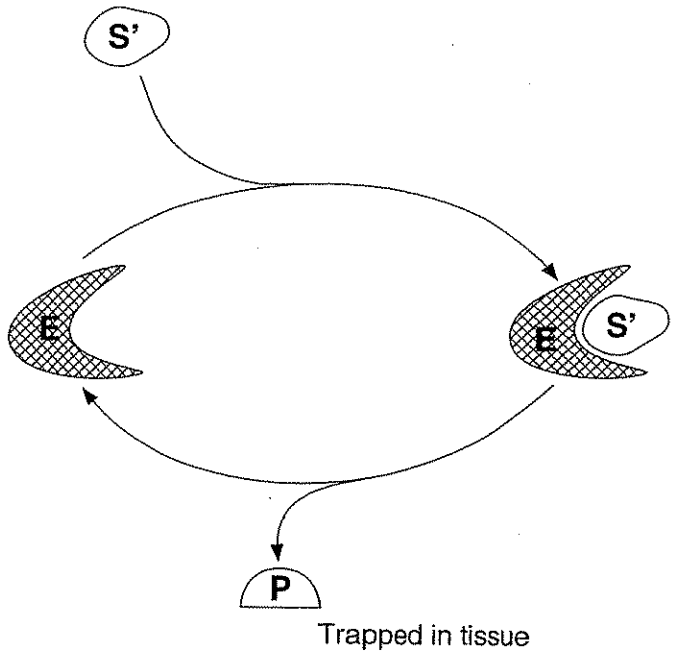


**FIGURE 4-3.** Diagrammatic representation of the enzyme (E)-mediated transformation of a molecular imaging probe (S′) into a product (P) that is trapped in tissue. An enzyme catalyzes a large number of molecular transformations amplifying the signal from the labeled end product of the reaction.

of DNA replication the utilization of which is based on the specific mammalian thymidine kinase-mediated phosphorylation to its 5′-phosphate.

### *Probing enzyme function*

In regards to structural requirements, enzyme-mediated probes are the ones with the strictest molecular constraints. Since enzymes have evolved over a period of millions of years, they have developed structural specificity for their substrates and have—for the most part—limited specificity to accommodate major modifications to the original substrate. Consider that enzymes are designed by evolution to accelerate chemical reactions decreasing the activation of the free energy barrier (G) between their natural substrate and product (Figure 4-4).

For a general reaction:

$$A + B \rightleftarrows C + D \tag{4-1}$$

there are two ways to accelerate its rate: (1) by an increase in temperature (T), which increases motion and the probability for molecules to enter the transition state; and (2) by means of a catalyst (enzyme). By combining transiently with the reactants (e.g., A and B), the enzyme will lower the transition state energy for the reaction to occur. To understand this effect, we need to look at the fundamental relationship between a free energy change ($\Delta G$) of a chemical reaction and its equilibrium constant (K), that is established as:

$$\Delta G = \Delta G^\circ + RT \ln \frac{[C][D]}{[A][B]} \tag{4-2}$$

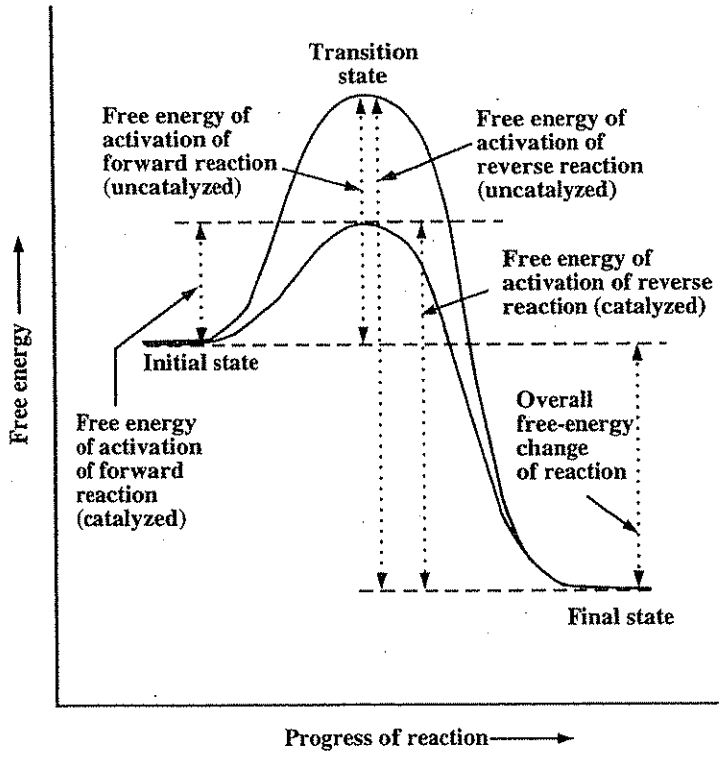


FIGURE 4-4. Energy diagram for a chemical reaction—catalyzed and uncatalyzed.

where R is the gas constant, T the absolute temperature and [A], [B], [C], and [D] the molar concentrations of solutes and, thus, $[C][D]/[A][B] = K$ (equilibrium constant) and $\Delta G^\circ$ is the standard free energy change of the reaction (e.g., at a concentration of 1 mol/L). At equilibrium, $\Delta G$ should be zero; then from Equation 4-2,

$$\Delta G^\circ = -RT \ln K \tag{4-3}$$

**EXAMPLE 4-1**

The estimated free energy of activation $\Delta G$ for the uncatalyzed and catalyzed (by catalase) decomposition of hydrogen peroxide at 20°C is 18 kcal/mol and 7 kcal/mol, respectively. How much catalase accelerates the rate of the reaction?

**ANSWER**

In Equation 4-3 the gas constant $R = 1.98 \times 10^{-3}$ kcal/mol and $T = 293°K$; thus, $\Delta G^\circ = -1.33 \log K$.

Since the $\Delta G^\circ$ difference between catalyzed (7 kcal/mol) and uncatalyzed reactions (18 kcal/mol) at 20°C is 11 kcal/mol, then:

$$\Delta G^\circ = -11 \text{ kcal/mol} = -1.33 \log K$$

$$\therefore \log K = \frac{11}{1.33} = 8.24$$

Then, the reaction rate for the decomposition of peroxide increases $10^8$-fold when the reaction is catalyzed by catalase.

**EXAMPLE 4-2**

The lowering of the energy of activation ($\Delta G$) explains enzymatic catalytic power, but how is this catalytic feat accomplished?

**ANSWER**

Enzymes are composed of amino acid residues forming chains (polypeptide chains) allowing free rotations about C—C and C—N bonds at their backbone. These amino acid residues can directly interact with water molecules in a complex fashion, in general forming hydrogen bonds with: 1) charged groups in the protein; 2) polar, uncharged groups (e.g., carbonyl groups); and hydrogen bonds 3) organized around nonpolar protein residues. These protein-water interactions are very dynamic in nature with almost 80% to 90% of the protein backbone involved, resulting in protein motions from very short (femtoseconds) to slow (milliseconds-seconds).

Enzyme interactions with the solvent cannot be separated from enzyme-substrate interactions. The solvent, water, is always present as the third component of binding and, therefore, enzyme-substrate interactions are also a very dynamic process. Therefore, the multiplicity of interactions between enzyme, substrate, and solvent result not in one but in a large number of substates that are close in energy. As a result, the description of the act of enzyme catalysis (e.g., transforma-

tion of the substrate into a product at the enzyme binding site) is attributable to the structural mobility of the enzyme-substrate complex and its consequence in lowering the energy of the reaction. Upon binding, the substrate displaces the nonspecific presence of water at the binding site in a continuously interactive way. Indeed, enzymes are not static but dynamic, constantly shaking structures. This motion induces transient strains in the substrate resulting in enzyme substates favoring transformation of the substrate into a product.[5]

Let's analyze the principles of enzyme kinetics to understand the importance of some concepts in molecular imaging probe design and utilization:

As an oversimplification of the concepts stated above, we can say that enzyme reactions typically consist of two steps: 1) formation of the enzyme-substrate complex (ES) and 2) decomposition of ES with formation of product (P).

$$E + S \underset{k_2}{\overset{k_1}{\rightleftarrows}} ES \xrightarrow{k_3} E + P \tag{4-4}$$

The rate of [ES] formation is determined by the difference between reactions leading to its formation and reactions leading to its disappearance:

$$d\frac{[ES]}{dt} = k_1[E][S] - k_2[ES] - k_3[ES] \tag{4-5}$$

Steady-state equilibrium assumes the concentration of [ES] is constant:

$$d\frac{[ES]}{dt} = 0 \tag{4-6}$$

To solve the equations, one should express them in terms of experimentally measurable quantities. For example:

$$[E_o] = [E] + [ES] \tag{4-7}$$

where $E_o$ = initial or total enzyme concentration that is measurable.

Therefore, combining Equations 4–3 and 4–5 under conditions of steady-state equilibrium render:

$$k_1([E_o] - [ES])[S] = (k_2 + k_3)[ES]$$

Upon rearrangement:

$$[ES](k_2 + k_3 + k_1[S]) = k_1E_o[S]$$

Solving for [ES] after dividing for $k_1$:

$$[ES] = \frac{E_o[S]}{K_m + [S]} \tag{4-8}$$

where $K_m = \frac{k_2 + k_3}{k_1}$ = Michaelis constant. The rate constants $k_1$, $k_2$, and $k_3$ control the formation and decomposition of [ES].

Thus, the velocity (V) of the enzymatic reaction is:

$$V = \frac{dP}{dt} = k_3[ES] = \frac{k_3[E_o][S]}{K_m + [S]} \tag{4-9}$$

When the enzyme is saturated, then the enzyme is mostly as the enzyme-substrate complex [ES] and $k_3[Eo]$ = maximal velocity of the reaction (Vm). The constant $k_3$ is also named $k_{cat}$ (catalysis constant), representing the rate of decomposition of the enzyme-substrate complex [ES].

Thus, Equation 4-9 becomes:

$$V = \frac{V_m[S]}{K_m + [S]} \tag{4-10}$$

also called the Michaelis–Menten equation.

Thus, $k_{cat}/K_m$ or $V_m/K_m$ is a measure of the enzymatic catalytic efficiency. Therefore, in enzymatically catalyzed reactions, the formation and rate of decomposition of the enzyme-substrate complex to form product are essential parameters to determine the ability of a particular substrate [S] to be transformed into product [P].

**EXAMPLE 4-3**

How is the principle of enzyme kinetics applied to a kinetic determination made with PET?

**ANSWER**

The principle of competitive kinetics applies when two competing reactions between two different substrates are taking place with the same enzyme (i.e., glucose and $FDG_6$ with hexokinase).

For the endogenous substrate:

$$E + [S] \underset{k_2}{\overset{k_1}{\rightleftarrows}} [ES] \xrightarrow{k_3} E + [P]$$

For the competitive substrate:

$$E + [S'] \underset{k_2'}{\overset{k_1'}{\rightleftarrows}} [ES'] \xrightarrow{k_3'} E + [P']$$

Under the steady-state assumption, $d\frac{[ES]}{dt} = 0$, thus, formation of [ES] is determined by:

$$[ES] = \frac{k_1}{k_2 k_3}(E_o - [ES] - [ES'])[S] \tag{4-11}$$

being $E_o$ = total enzyme concentration and $k_1/k_2 + k_3 = 1/K_m$.

Similarly,

$$[ES'] = \frac{k_1'}{k_2' K_3'}(E_o - [ES] - [ES'])[S'] \tag{4-12}$$

where $k_1'/k_2' + k_3' = 1/K_m'$.

Thus:

$$[ES]K_m = E_o[S] - [ES][S] - [ES'][S] \tag{4-13}$$

and

$$[ES']K_m' = E_o[S'] - [ES][S'] - [ES'][S'] \tag{4-14}$$

Therefore,

$$[ES](K_m[S]) = E_o[S] - [ES'][S] \tag{4-15}$$

and

$$[ES] = \frac{E_o[S] - [ES'][S]}{K_m + [S]} \tag{4-16}$$

Replacing [ES] in Equation 14:

$$[ES']K_m' = E_o[S'] - \frac{E_o[S] - [ES'][S]}{K_m + [S]}[S'] - [ES'][S']$$

$$= [E_o][S'] - \frac{E_o[S][S']}{K_m + [S]} + \frac{[ES'][S][S']}{K_m + [S]} - [ES'][S'] \tag{4-17}$$

Rearranging terms:

$$[ES']\left(K_m' - \frac{[S][S']}{K_m + [S]} + [S']\right) = E_o[S'] - \frac{E_o[S][S']}{K_m + [S]} \tag{4-18}$$

Solving [ES']:

$$[ES'] = \frac{[E_o][S'] - \dfrac{E_o[S] + [S']}{K_m + [S]}}{K_m' - \dfrac{[S][S']}{K_m + [S]} + [S']} \tag{4-19}$$

Rearranging terms:

$$[ES'] = \frac{E_o[S'](K_m + [S]) - E_o[S][S']}{K_m'(K_m + [S]) - [S][S'] + [S'](K_m + [S])}$$

$$= \frac{E_o K_m[S']}{K_m'K_m + K_m'[S] + K_m[S']}$$

$$[ES'] = \frac{\dfrac{E_o}{K_m}[S']}{1 + \dfrac{[S]}{K_m} + \dfrac{[S']}{K_m'}} \tag{4-20}$$

Therefore, the velocity ($V'$) of the reaction with a competitive substrate ($S'$) is:

$$V' = k_c'[ES'] = \frac{\dfrac{k_c'E_o}{K_m}[S']}{1 + \dfrac{[S]}{K_m} + \dfrac{[S']}{K_m'}} \tag{4-21}$$

Since $V'_m = k_c' E_o$,

$$V' = \frac{\dfrac{V'_m}{K_m'}[S']}{1 + \dfrac{[S]}{K_m} + \dfrac{[S']}{K_m'}} \tag{4-22}$$

If the competitive substrate concentration is very low ([S′]≪[S]), as is always the case with PET determinations where the molecular imaging probe is used in tracer concentrations, Equation 4-22 can be simplified further:

$$V' = \frac{\frac{V'_m}{K_m'}}{1 + \frac{[S']}{K_m}}[S'] \tag{4-23}$$

that is the reaction rate measured by PET:

$$V' = k_3'(PET)[S'] = \frac{\frac{V'_m}{K_m'}}{1 + \frac{[S]}{K_m}}[S'] \tag{4-24}$$

where k3′ (PET) is the rate constant of the enzyme reaction.

If we divide by $V$, or the original rate of the endogenous process unaffected by the presence of the tracer [S′]:

$$\frac{V'}{V} = \frac{\frac{V'_m K_m'}{1 + [S]/K_m'[S']}}{\frac{V_m K_m}{1 + [S]/K_m}[S]} \tag{4-25}$$

Rearranging terms:

$$\frac{V'}{V} = \frac{V_m'/K_m'[S']}{V_m/K_m[S]} \tag{4-26}$$

Therefore, $V$, the rate of the endogenous reaction to be measured (i.e., local metabolic rate for glucose, LMRGlc) with the molecular imaging probe (i.e., FDG) and PET combining Equations 4-24 and 4-26 is:

$$V = k_3'(PET)[S']\frac{V_m/K_m[S]}{V_m'/K_m'[S']}$$

Thus:

$$V = k_3'(PET)\frac{V_m/K_m}{V_m'/K_m'}[S] \tag{4-27}$$

In the case of glucose metabolic rate determinations with FDG, $V$ = LMRGlc, [S] = plasma glucose concentration and $\frac{V_m'/K_m'}{V_m/K_m}$ = lumped constant (LC) indicating the ratio of catalytic efficiency between the imaging probe and the endogenous substrate.[6] Thus, LC is derived from the principle of competitive kinetics to convert the measured reaction rate of a substrate analog to the reaction rate of the natural substrate. Unless this ratio is known, no absolute determination of the endogenous process can be made. It should be noted, however, that the LC does vary with the species of animal (Table 4-1)[7–13] and also changes in pathophysiological states, (e.g., severe hypoglycemia).[14]

**TABLE 4-1. Values of the FDG Lumped Constant in Several Species**

| *Species* | *Mean ± SD* | *Reference* |
|---|---|---|
| Albino rat | | |
| Conscious | 0.464 ± 0.099[a] | Sokoloff, 1986[7] |
| Anesthetized | 0.512 ± 0.118[a] | Sokoloff, 1986[7] |
| Conscious (5% $CO_2$) | 0.463 ± 0.122[a] | Sokoloff, 1986[7] |
| Combined | 0.481 ± 0.119 | Sokoloff, 1986[7] |
| Rhesus monkey | | |
| Conscious | 0.344 ± 0.095 | Sokoloff, 1986[7] |
| Cat | | |
| Anesthetized | 0.411 ± 0.013 | Sokoloff, 1986[7] |
| Dog (beagle puppy) | | |
| Conscious | 0.558 ± 0.082 | Sokoloff, 1986[7] |
| Sheep | | |
| Fetus | 0.416 ± 0.031 | Sokoloff, 1986[7] |
| Newborn | 0.382 ± 0.024 | Sokoloff, 1986[7] |
| Mean | 0.400 ± 0.033 | Sokoloff, 1986[7] |
| Human | | |
| Conscious | 0.568 ± 0.105 | Sokoloff, 1986[7] |
| Conscious | 0.418 ± 0.058 | Huang et al, 1980[8] |
| Conscious | 0.520 ± 0.028 | Reivich et al, 1985[9] |
| Conscious | 0.660 ± 0.170[b] | Hasselbalch et al, 1997[10] |
| Conscious | 0.670 ± 0.210[c] | Hasselbalch et al, 1997[10] |
| Conscious | 0.810 ± 0.150 | Hasselbalch et al, 1998[11] |
| Conscious | 0.860 ± 0.140 | Spence et al, 1998[12] |
| Conscious | 0.670 ± 0.170 | Wu et al, 2001[13] |

[a]No statistically significant difference between normal conscious and anesthetized rats ($0.3 < p < 0.4$) and conscious rats breathing 5% $CO_2$ ($p > 0.9$); [b]Steady state; [c]Bolus injection.

When the principle of competitive enzyme kinetics is used with PET, the molecular imaging probe (i.e., FDG) will compete with the endogenous substrate (i.e., glucose) for the same sites at the catalytic enzyme (e.g., hexokinase). This competition between the newly designed imaging probe and the endogenous substrate for the same enzyme site immediately indicates that the imaging probe should have very favorable kinetic characteristics to trace the process under study. If the imaging probe has low Vm′ and high Km′ (low Vm′/Km′), it will compete unfavorably with the endogenous substrate, with two consequences: 1) a reduction in the probability of yielding a metabolic trapping product of the labeled analog and 2) as a result, a low PET signal. Therefore, favorable enzyme kinetic characteristics of the imaging probe permit competition with the endogenous substrate for successful formation of the radiolabeled trapping product leading to accumulation of the labeled product—an essential consideration in designing enzyme-mediated molecular imaging probes.

### *Using substrate analogs of enzyme function*

To further understand the question of why knowledge of the target molecule in tissue is important, this chapter will analyze the example of hexokinase and the successful use of a radiolabeled substrate analog of enzyme function, FDG, as a molecular imaging probe to estimate local rates of glucose metabolism. FDG was found to retain the transport and enzymatic characteristics of 2-deoxy-D-glucose. Its utilization for the noninvasive determina-

tion of LMRGlc is then based on the general biochemical principle developed by Sokoloff et al[6] with [C-14]2-deoxy-D-glucose. Fluorination of carbon-2—that is, the replacement of the OH group in the 2-position of D-glucose with a fluorine—is successful for at least two reasons: First, it respects the steric characteristics of D-glucose without any substantial distortion in geometry, which is a requirement for preservation of its needed activity with hexokinase; and, second, it predictably assures that fluorodeoxyglucose-6-phosphate (FDG-6-P), the product of the hexokinase-mediated phosphorylation of FDG, will not be susceptible to further metabolism within the time-frame of the imaging determination (e.g., typically 45 min). The reason is that the next reaction in the glycolytic pathway after hexokinase is the freely reversible isomerization of glucose-6-phosphate to fructose-6-phosphate, in effect, a rearrangement of the carbonyl group from C-1 to C-2. The enzymatic transformation imposes structural and geometric requirements in the substrate that cannot be met by FDG due to the presence of fluorine substitution on carbon 2. All these factors make the accumulation of radioactivity in the use of FDG very specific to the measurement of glucose metabolic rates. At pharmacological doses, FDG can block phosphorylation of glucose due to inhibition of hexokinase by FDG-6-P. This mechanism was observed early when 2-deoxy-D-glucose was originally introduced as a therapeutic agent to inhibit glycolysis in tumors. Because of the high-specific activity of FDG (Chapter 3), there are no significant mass action effects of FDG-G-P on hexokinase when a PET determination is performed.

Consequently, the time-dependent accumulation of radioactivity as FDG-6-P is proportional to the rate of the hexokinase-mediated reaction in tissue. This biochemical trick, referred to as the principle of metabolic trapping, permits the biochemical isolation of the hexokinase reaction, whose rate under steady-state conditions is equal to the glycolysis rate or LMRGlc assuming no significant glycogen formation or breakdown. It has been estimated that only 3% of glucose is metabolized via the pentose phosphatase shunt, at least in normal rat brain.[15] Moreover, the radiofluorinated glucose analog is a poor substrate of glucose-6-phosphate dehydrogenase,[16] the first enzyme in the pentose phosphate shunt. Therefore, this pathway seems to contribute only minimally to the measure of LMRGlc. Similarly, the influence of the highly compartmentalized glucose-6-phosphatase to hydrolyze back FDG-6-P is low within the experimental period of the tomographic determination (e.g., 45 min)[17] (Chapter 2). Thus, FDG provides a measure of the rate of hexokinase-mediated glycolysis, independent of all subsequent reactions in the glycolytic pathway.

The *in vivo* kinetic properties of FDG as a substrate for hexokinase are in accord with the mechanism of hexokinase binding to its substrate and ATP to induce phosphorylation at carbon-6. In the design of a radiolabeled imaging probe targeting hexokinase to measure local glucose metabolic rates, it is important to know that hexokinase is particularly insensitive to modifications at carbon 2, including stereochemical modifications. In that regard, FDG and 2-deoxy-2-fluoro-D-mannose (FDM), which only differ in the fluorine atom configuration (e.g., the fluorine substitution can have two possible arrangements) at carbon-2, are both good substrates for hexokinase. By contrast, 1-fluoro-, 3-fluoro- and 4-fluorodeoxy-D-glucoses are poor substrates for hexokinase (Table

**TABLE 4-2. Experimentally Determined Kinetic Constants of Fluorohexoses with Hexokinase**

| Compound | $K_m$ (mM) | Relative $V_{max}$ | $K_m$ $MgATP^{2-}$ (mM) | Calculated K′m | Experimental K′m |
|---|---|---|---|---|---|
| | | | | $K_m$ (glucose) | $K_m$ (glucose) |
| D-Glucose | 0.17 | 1.00 | 0.20 | 1 | 1 |
| 2-Deoxy-D-*arabino*-hexose | 0.59 ± 0.11 | 0.85 | 0.36 ± 0.11 | — | — |
| 2-Deoxy-2-fluoro-D-glucose | 0.19 ± 0.03 | 0.50 | 0.26 ± 0.05 | 1.14 | 1.36 ± 0.37 |
| 2-Deoxy-2-fluoro-D-mannose | 0.41 ± 0.05 | 0.85 | 0.66 ± 0.25 | 2.46 | 0.86 ± 0.75 |
| 2-Deoxy-2,2-difluoro-D-*arabino*-hexose | 0.13 ± 0.02 | 0.53 | 0.21 ± 0.02 | 0.78 | 0.91 ± 0.47 |
| 3-Deoxy-3-fluoro-D-glucose | 70 ± 30[a] | 0.10 | 2.3 ± 0.3[b] | — | — |
| 4-Deoxy-4-fluoro-D-glucose | 84 ± 30[a] | 0.10 | 1.9 ± 0.1[c] | — | — |
| 2-Chloro-2-deoxy-D-glucose | 2.1 ± 0.6 | 0.54 | 0.97 ± 0.33 | 12.6 | 9 ± 10 |

*Source*: Reprinted from Bessell et al.,[18] with permission from Biochemical Journal, © The Biochemical Society.

[a]Concentration of ATP, 4.1 mM. [b]Concentration of 3-deoxy-3-fluoro-D-glucose, 10 mM.

[c]Concentration of 4-deoxy-4-fluoro-D-glucose, 10 mM.

*Note*: Compounds that are not substrates: α-D-glucopyranosyl fluoride, β-D-glucopyranosyl fluoride, 2-O-methyl-D-glucose, 2,2-dichloro-2-deoxy-D-*arabino*-hexose, 2-deoxy-2-fluoro-D-galactose, 2,3-anhydro-D-mannose (kindly provided by Professor J. G. Buchanan), 2-chloro-2-deoxy-D-mannose, 2-O-methyl-D-mannose. Compounds that are not inhibitors: α-D-glucopyranosyl fluoride, β-D-glucopyranosyl fluoride, 2-deoxy-2-fluoro-D-galactose, 2-deoxy-2,2-dichloro-D-*arabino*-hexose, 2,3-anhydro-D-mannose. Compounds that are inhibitors: 2-O-methyl-D-glucose ($K_I$ 60mM), 2-O-methyl-D-mannose ($K_I$ 7mM). Values are means ± SEM.

4-2).[18] Therefore, in the design of a successful molecular imaging probe, the issue is not only whether a radiolabeled fluorine atom can be introduced on a specific substrate, but also how to meet the biochemical requirements imposed by the target enzyme/receptor.

**EXAMPLE 4-4**

Is it possible to use other radiolabeled halogenated (i.e., I-123; Br-75) glucose analogs to adapt the same concept described above to single-photon emission tomography?

**ANSWER**

In most cases, it is easier to introduce synthetic iodine, bromine, or chlorine than fluorine to a given site in a molecule. Then it is not a question of whether the synthesis of halogenated probes is possible, but whether radiohalogenated probes, other than radiofluorinated probes, are useful for the intended purpose. Beyond the excellent physical qualities of fluorine-18 as a positron emitter, e.g., 97% positron decay mode, a convenient half-life (109.72 min), a short positron range (Chapter 1), and the capability of being prepared with high-specific activity, its importance resides in the fact that fluorine is the second smallest substituent, closely mimicking hydrogen in geometric requirements (the van der Waal's radii of fluorine and hydrogen atoms are very similar, 1.35 and 1.2 Å, respectively). The van der Waals radius of a group or atom is a measure of its size, and the larger the atom, the higher the probability of unfavorable interaction with another group or atom at the enzyme binding site. If this occurs—if, in other words, the electron clouds begin to penetrate each other—the

interaction becomes repulsive. As a result, one can expect that C-F analogs will closely mimic the biological behavior of C-H derivatives. The high fluorine of electronegativity, however, introduces a polarity more akin to a hydroxyl substituent.[19] This explains why, when compared with glucose which contains an OH group at the 2 position, FDG binding affinity with hexokinase, as well as the chemical reactivity of the transition state intermediate during phosphoryl transfer, is not drastically affected (e.g., Vm'/Km' and Vm/Km are similar; Table 4-2). All other 2-radiohalogenated deoxyglucoses would not meet these criteria because of the larger van der Waal's radii of the other halogens (Cl, Br, and I). The geometric constraints imposed by these radiohalogenated deoxyglucose analogs drastically reduce their binding affinity with the enzyme (hexokinase). For example, the Km of 2-chloro-2-deoxy-D-glucose for hexokinase is 0.97 mM, about 5-fold higher than that of FDG.[20] For larger halogens, the apparent affinity for hexokinase drops even further. As a result, 2-radiohalogenated deoxyglucoses, other than FDG, cannot be effectively used as molecular imaging probes for LMRGlc.

### *Molecular imaging probes targeting tumor enzymes*

The principle of the FDG method has been applied to the investigation of the biochemistry of cancer. It is currently applied extensively to the diagnosis and staging of the disease (Chapter 5). The knowledge obtained with FDG is centered on energy utilization by tumor cells *in vivo*, as a source of energy (e.g., adenosine triphosphate or ATP). Recently, approaches to target enzymes involved in biosynthetic processes in the tumor have been developed. The two most relevant examples are the development and use of: 1) fluorine-18-labeled 3'-fluoro-3'-deoxythymidine ([F-18]FLT) as a probe of DNA replication and, therefore, cell replication, targeting mammalian thymidylate kinase (TK); and 2) carbon-11-labeled choline and fluorine-18 labeled choline analogs to target choline kinase. Both enzymes are overexpressed in tumor tissue. Other approaches targeting tyrosine kinases in tumors are under development.

#### *3'-[F-18]FLUORO-3'-DEOXYTHYMIDINE ([F-18]FLT)*

Using [F-18]FLT as an imaging probe of DNA replication is based on early work on the use of 3'-fluoro-3'-deoxythymidine[21] as a candidate for an anti-AIDS drug in clinical trials.[22] Incorporation of FLT via mono-, di-, and triphosphates into the DNA of MT4 cells and other cell lines was demonstrated.[23] The ability of FLT to incorporate into DNA resides in the efficiency of its triphosphate, formed intracellularly following the thymidine kinase (TK)-mediated synthesis of its monophosphate, as a substrate of DNA polymerases.[24] It appears that within the time of the PET determination, however, [F-18]FLT-5'-monophosphate is the main product accumulating in tissue (Figure 4-5).

F-18 FLT[25,26] has been used in animal models and humans[27] and has been shown to be effective in the visualization of primarily nonsmall cell lung cancer and brain tumors as well as normal highly proliferating tissues such as bone marrow (Figure 4-6). [F-18]FLT has excellent properties as a molecular imaging probe in that it has specificity for mammalian TK and is essen-

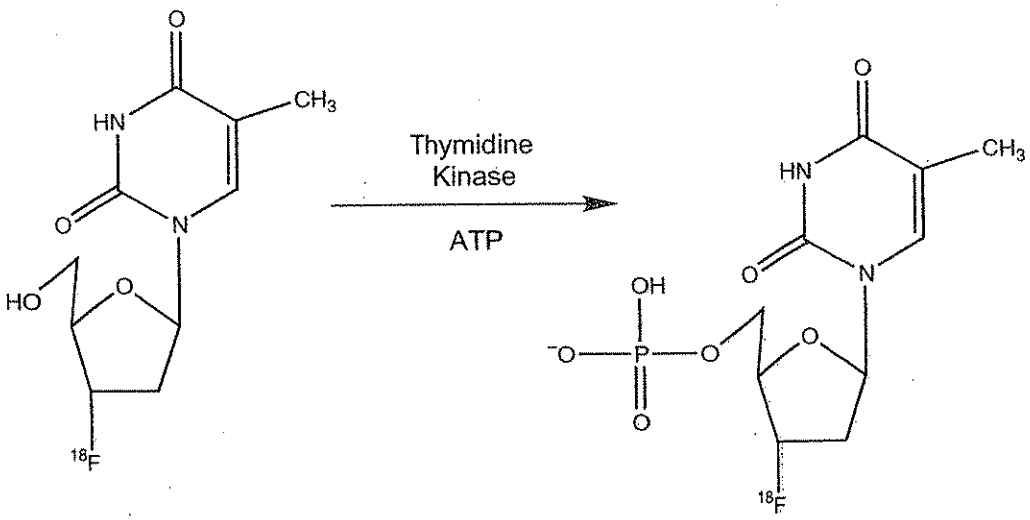


**FIGURE 4-5.** Description of the thymidine kinase-mediated phosphorylation of [F-18]FLT into its 5′-monophosphate that is metabolically trapped in tissue within the time of the experimental determination with PET (i.e., ≤ 2 h). With longer exposure times, the monophosphate would be subsequently phosphorylated by cellular kinases to the di- and tri-phosphate, and the latter incorporated into DNA.

tially not metabolized *in vivo* in dogs. However, it appears to have increased glucuronidation in humans, as evidenced by its accumulation in hepatocites.[27]

**EXAMPLE 4-5**

What would be necessary to know to quantify the mammalian TK-mediated phosphorylation of [F-18]FLT?

**ANSWER**

Similar to FDG, the use of [F-18]FLT is based on the principle of metabolic trapping mediated by mammalian TK (Figure 4-6). Because trapping is due to the initial phosphorylation of [F-18]FLT mediated by mammalian TK to [F-18]FLT 5′-monophosphate, a similar 3-compartment model can be used for the determination of $k_3$ (PET), or the rate of accumulation of the probe in DNA. However, the determination of the absolute rate of DNA replication would require knowledge of the concentration of thymidine in tissue (i.e., tumor or bone marrow), and the determination of the transport and enzyme-mediated rate constants for [F-18]FLT and thymidine to act as substrates with TK (i.e., $V_{max}/K_m$ and $V_{max}/K_m$, respectively; Equation 4-27, p. 281). This information is not yet available for the substrate analog. Thus, [F-18]FLT is currently used only semiquantitatively to assess relative alterations in DNA replication.

*RADIOLABELED CHOLINE AND FLUORINATED ANALOGS*

These molecular imaging probes are used to target choline kinase, an enzyme elevated in tumor cells. These molecular imaging probes are particularly useful in prostate cancer because of their ability to be rapidly trapped in the prostate can-

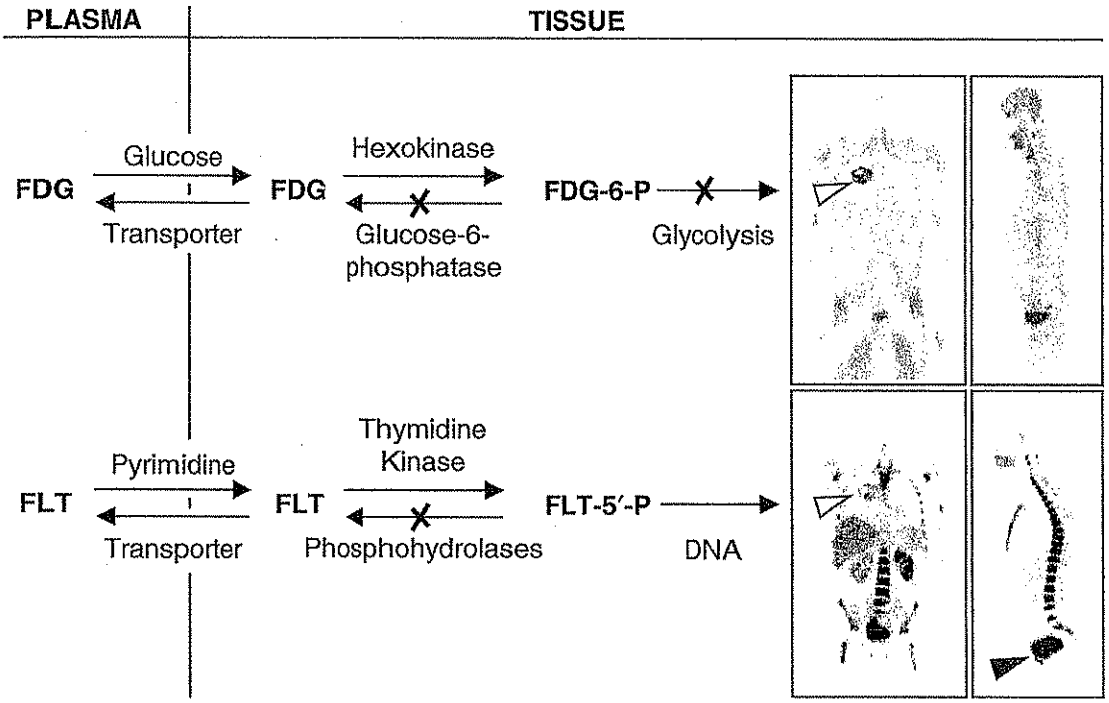


**FIGURE 4-6.** Tracer kinetic models for FDG and [F-18]FLT based on their biochemical similarities as molecular imaging probes. Arrows show forward and reverse transport between plasma and tissue and phosphorylation and dephosphorylation. Both FDG and [F-18]FLT phosphates are not significant substrates for dephosphorylation or further metabolism at normal imaging times of 40 min to 60 min after injection. Images are 6-mm-thick longitudinal tomographic sections of a patient with a lung tumor (arrows) that has high glucose metabolism and DNA replication. The rest of the images show normal distribution of glucose utilization and DNA replication, exceptions being the clearance of both tracers to the bladder (arrowhead) and in the case of [F-18]FLT glucuronidation by hepatocytes in the liver.

cer cells, coupled with their slow excretion rate via the kidney to the bladder, which can obscure the prostate gland. This results in clear visualization of primary prostate cancer, proximal lymphatic nodes, and local metastasis in humans, because no or little activity accumulates in the bladder in the first 10 minutes after intravenous administration of the radiolabeled probe (Chapter 5; Figure 4-7).[28]

Carbon-11 (methyl)-labeled choline[29] was utilized in the detection of brain tumors[30,31] prostate cancer,[32] and esophageal carcinoma[33] with good results. The target enzyme is choline kinase[34] that not only takes choline as a substrate but has sufficient binding flexibility at the binding site pocket to phosphorylate other analogs (Table 4-3).[34] The enzyme transforms choline into its phosphorylated form, which is then incorporated into membrane components of tumor cells (i.e., phospholipids). As a result of this essential activity in tumor cell proliferation, the enzyme has also been considered as a therapeutic target.[35]

Choline kinase seems to tolerate modifications in one of the methyl groups of choline well. Fluoromethyl- and fluoroethyl-choline-substituted analogs are good substrates for the enzyme (e.g., compare $V_m/K_m$ to that of choline). Initial results in prostate cancer patients with an F-18-labeled fluoromethylcholine analog seem to confirm these expectations *in vivo*. It appears, however, that excretion via kid-

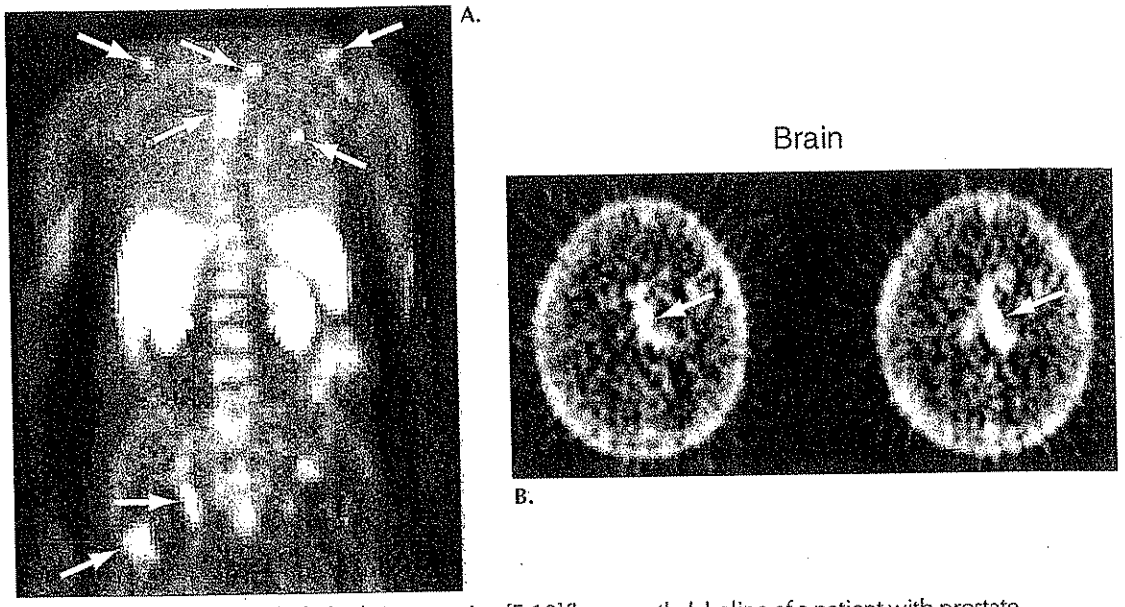


**FIGURE 4-7.** Whole-body image using [F-18]fluoromethylcholine of a patient with prostate cancer taken 5 min to 8 min after injection of the probe. A) Notice the presence (arrows) of tumor metastasis in the pelvic area and upper thorax, as well as the lack of activity in the bladder. B) Metastasis (arrows) is also observed in the brain of this patient. At later times, the radiolabeled probe is excreted via the kidney and fills the bladder.

ney is increased with the fluorinated analog when compared with C-11 choline,[28] which essentially shows no accumulation of activity in the bladder.

**EXAMPLE 4-6**

Do choline derivatives meet the necessary requirements for quantitation of choline kinase activity?

**ANSWER**

Initial studies have shown that choline and derivatives are fairly specific for the target enzyme, choline kinase. However, their significant peripheral metabolism *in vivo* may complicate the formulation of tracer kinetic modeling for quantitation of choline activity as a marker of phospholipid synthesis in the target tissue (e.g., tumor). Regardless, the qualitative use of labeled choline analogs to identify accelerated increases in phospholipid synthesis, that can be increased more than 10-fold in tumors, has been demonstrated. Moreover, as indicated above for [F-18]FLT, for quantification it is necessary to know: 1) the concentration of the endogenous substrate, choline (preferentially in the tissue target); and 2) the kinetic characteristics ($Vm''/Km''$) of the radiolabeled probe. Vm/Km of choline are known.[34] It is obvious that the use of C-11 choline would simplify the quantification process because in Equation 4-27 $Vm/Km/Vm''/Km'' = 1$. However, whenever possible, fluorinated choline analogs are more attractive for human use because of the longer half-life of F-18 compared with that of C-11.

**TABLE 4-3. Acyclic, Alkyl Analogs of Choline as Substrates of Yeast Choline Kinase**

| Compound | | | | | Relative $V_{max}$* | Apparent $K_m$ ($\mu M$) |
|---|---|---|---|---|---|---|
| Number | $R_1$ | $R_2$ | $R_3$ | $R_4$ | | |
| 1a | $-CH_3$ | $-CH_3$ | $-CH_3$ | $-CH_3CH_2OH$ | 100 (100) | 18 ± 2 |
| b | $-H$ | $-H$ | $-H$ | $-CH_2CH_2OH$ | −(5 ± 1) | — |
| c | $-H$ | $-H$ | $-CH_3$ | $-CH_2CH_2OH$ | 24 ± 2 (22 ± 1) | 1107 ± 273 |
| d | $-H$ | $-CH_3$ | $-CH_3$ | $-CH_2CH_2OH$ | 37 ± 2 (37 ± 2) | 66 ± 1 |
| e | $-CH_2CH_3$ | $-CH_3$ | $-CH_3$ | $-CH_2CH_2OH$ | 110 ± 6 (100 ± 5) | 17 ± 1 |
| f | $-CH_2CH_2CH_3$ | $-CH_3$ | $-CH_3$ | $-CH_2CH_2OH$ | 116 ± 5 (80 ± 4) | 33 ± 4 |
| g | $-CH_2CH_2CH_2CH_3$ | $-CH_3$ | $-CH_3$ | $-CH_2CH_2OH$ | −(8 ± 2) | — |
| h | $-CH_2CH_3$ | $-CH_2CH_3$ | $-CH_3$ | $-CH_2CH_2OH$ | 96 ± 8 (82 ± 3) | 68 ± 15 |
| i | $-CH_2CH_3$ | $-CH_2CH_3$ | $-CH_2CH_3$ | $-CH_2CH_2OH$ | 38 ± 5 (21 ± 3) | 652 ± 115 |
| j | $-CH_3$ | $-CH(CH_3)_2$ | $-CH(CH_3)_2$ | $-CH_2CH_2OH$ | −(7 ± 1) | — |
| k | $-CH_3$ | $-CH_3$ | $-CH_3$ | $-CH_2CH_2CH_2OH$ | 55 ± 4 (45 ± 2) | 117 ± 14 |
| l | $-CH_3$ | $-CH_3$ | $-CH_3$ | $-CH_2CH_2CH_2CH_2OH$ | −(< 3) | — |
| m | $-CH_3$ | $-CH_3$ | $-CH_3$ | $-CH_2CH(CH_3)OH$ | −(< 3) | — |
| n | $-CH_3$ | $-CH_3$ | $-CH_3$ | $-C(CH_3)_2CH_2OH$ | −(< 3) | — |
| o | $-CH_3$ | $-CH_3$ | $-CH_3$ | $-CH(CH_3)CH_2OH$ | 39 ± 4 (41 ± 1) | 443 ± 28 |

*Source*: Reprinted from Clary et al.,[34] with permission from Elsevier.

*Note*: Each analog was compared with choline at a constant (10 mM) substrate concentration and a fixed, saturating concentration of ATP and magnesium to give a relative initial rate (choline = 100). For those analogs with a relative initial rate greater than 25% of that of choline, a relative apparent $V_{max}$ and an apparent $K_m$ ( ± SEM) were also determined. Compounds 1m and 1o are racemic mixtures. Compound 1a is choline.

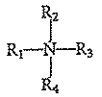


*The values within the parentheses report the relative rate ( ± SEM) of the reaction obtained at a fixed substrate concentration (10 mM).

## Probes based on stoichiometric binding interactions

### *Receptor-ligand binding: general principles*

These imaging probes are radiolabeled drug derivatives or analogs that bind with a high degree of specificity to: 1) receptor systems, 2) neurotransmitter presynaptic reuptake carriers, or 3) enzymes. Unlike probes based on enzyme-mediated transformations, these probes do not experience chemical modifications as a result of this interaction. There are many examples in the literature of these kinds of drug-mimicking probes that have permitted extensive evaluation of central neurotransmission and other biochemical processes with PET in health and disease (Table 4-4). In contrast with probes for enzyme-mediated reactions, trapping of receptor-mediated probes is the result of stoichiometric binding to the target site (Figure 4-8). This trapping of the molecular imaging probe (or receptor ligand) is related to its specificity for the target site, the number of target sites (Bmax), and its affinity (KD) for the same target. Because the number of target sites is limited (typically in the nanomolar concentration) in tissue and the binding is stoichiometric, binding specificity is highly dependent on the specific activity (Chapter 3) of the PET imaging probe. When the probe specific activity decreases (mass of cold or unlabeled component increases per unit amount of radioisotope), receptor site occupancy may reach saturation affecting the accuracy of the determination by lowering the ratio of specific-to-nonspecific binding and, thus, image contrast. On the other hand, this very important property of receptor sites can be exploited using these molecular imaging

**TABLE 4-4. Selected Imaging Probes and Their *In Vivo* Use with PET**

| *Imaging probe* | *Use* |
|---|---|
| 6-[F-18]Fluoro-L-dopa | Presynaptic dopaminergic function |
| 4-[F-18]Fluoro-L-m-tyrosine | Presynaptic dopaminergic function |
| 6-[F-18]fluoro-L-m-tyrosine | Presynaptic dopaminergic function |
| 2-[F-18]Fluoro-L-tyrosine | Protein synthesis, amino acid transport |
| [F-18]Long-chain fatty acids | $\beta$-Oxidation |
| [F-18]Misonidazole | Hypoxic cells |
| [F-18]N-Methylspiperone | D-2 Receptor |
| N-[F-18]Fluoroethylspiperone | D-2 Receptor |
| [F-18]Fluoroalkylbenzamides | D-2 Receptor |
| 4-[F-18]Fluorodexetimide | Muscarinic acetylcholine receptor |
| MPPF | 5-$HT_{1A}$ Receptor |
| N-[F-18]Fluoroethylketanserin | 5-$HT_2$ Receptor |
| [F-18]Setoperone | 5-$HT_2$ Receptor |
| [F-18]Altanserin | 5-$HT_2$ Receptor |
| 4-[F-18]Fluorofentanil | Opioid receptor |
| [F-18]3-Acetylcyclofoxy | Opioid receptor |
| [F-18]Fluoroethylflumazenil | Benzodiazepine receptor |
| 6-[F-18]Fluoronorepinephrine | Adrenergic nervous system |
| 5-[F-18]Fluorouracil | Tumor therapy control |
| 16$\alpha$-[F-18]Fluoroestradiol | Breast tumors |
| [F-18]FLT | DNA replication and cell proliferation |
| C-11- and F-18-labeled choline analogs | Phospholipid synthesis in tumors |

*Abbreviations:* D-2, dopamine2 receptor; FLT, 3'-deoxy-3'-fluorothymidine; $HT_2$, serotonin type 2 receptor; MPPF, 4-[F-18]fluoro-N-{2-[4-(2-methoxyphenyl)piperazin-1-yl]ethyl}-N-pyridin-2-ylbenzamide.

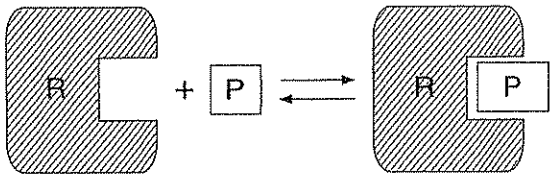


**FIGURE 4-8.** Schematic representation of the stoichiometric interaction of a molecular imaging probe (P) with a receptor (R). Similar interactions may exist with enzymes, mimicking enzyme inhibitor interactions commonly found with drugs.

probes to determine receptor occupancy by drugs [see Molecular Imaging in Drug Development (p. 310) and Chapter 2]. Therefore, PET imaging probes using receptors as targets should typically have very high-specific activity (1-10 Ci/$\mu$mol) to preclude mass effects during the *in-vivo* determination. This requirement can be met with probes for enzyme–mediated reactions, but is not critical. Enzyme-mediated probes can be successfully used even at specific activities 1,000 times lower (1-10 Ci/mmol) than the ones needed for receptor-mediated probes. Also, the binding affinity of these stoichiometric probes for their target should be high, typically in the nanomolar range. Low-binding affinities diminish the specificity of the determination because the measured radioactivity in tissue containing the receptor target may not be increased over that of tissue lacking receptors.[4A]

### *Imaging endogenous gene expression with radiolabeled oligonucleotides: a perspective from probe design*

Imaging approaches directed to gene expression involve either externally transferred genes into cells (transgenes) or endogenous genes (Figure 4-9). The imaging approach involves extending reporter gene techniques used in biology to PET using a PET reporter gene (PRG) and a PET reporter probe (PRP). The PRG–PRP approach has used either an enzyme or a receptor gene as PRG. PRP is, therefore, either an imaging probe that is a substrate of the PRG-enzyme or a probe that is a ligand that binds to the PRG-receptor. In both approaches, the PRG is incorporated into the genome of an adenovirus, which, following intravenous injection into the mouse tail vein, mainly localizes (> 90%) in the liver. Thus, using microPET technology (Chapter 1), it is possible to determine the location, magnitude, and temporal changes of gene expression. In either case, the principle of utilization follows the general discussion above [e.g., 1) probes based on enzyme-mediated transformations[36–39] and 2) probes based on stoichiometric binding interactions.[38,40]] A detailed description of the assays, strategies, and procedures is found in Chapter 2.

Endogenous gene expression is generally directed at the transcription of genes into messenger RNA (mRNA). Single-stranded mRNA is encoded with four bases: adenine (A), cytosine (C), guanine (G), and uracil (U). Specific sequences are targeted for imaging using radiolabeled antisense oligonucleotides (RASON) with a sequence complementary to a specific sequence on the target mRNA molecule. Complementarity is established with the specific pairing of A and U (or thymidine, T, in DNA molecules) and C with G (Figure 4-10). Then, the approach is based on stoichiometric binding of the radiolabeled imaging probe with an endogenous target molecule as described above.

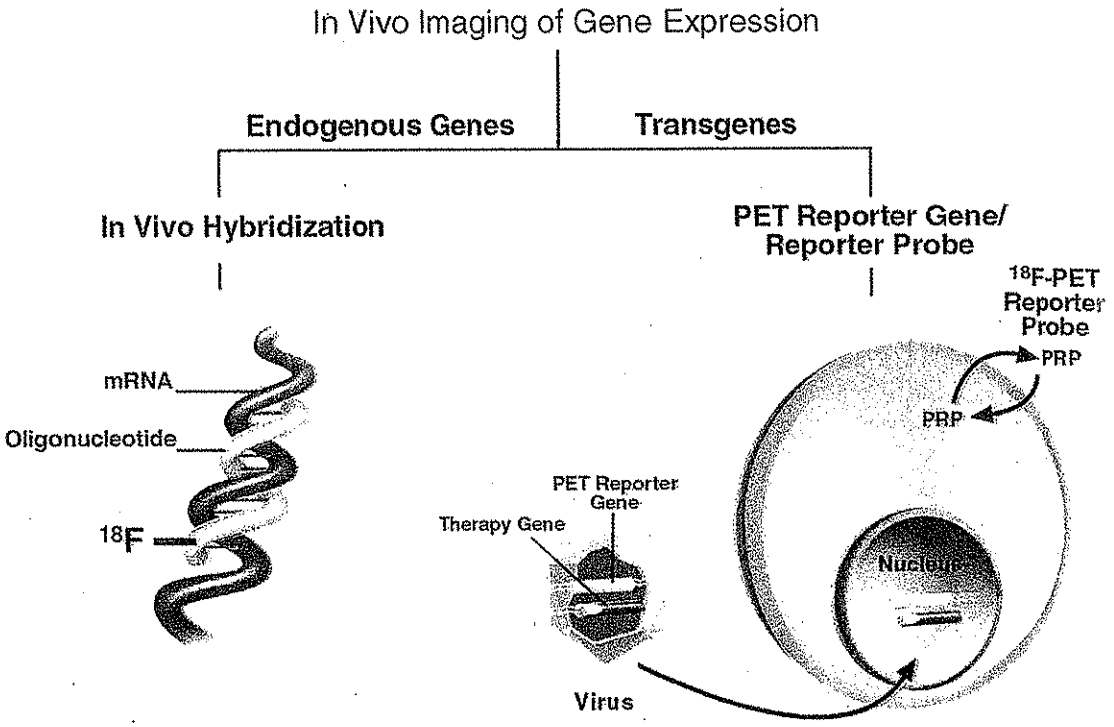


**FIGURE 4-9.** Two approaches to imaging gene expression *in vivo* with PET. The approach on the left images the expression of endogenous genes. *In situ* hybridization is translated to *in vivo* hybridization using F-18-labeled oligonucleotides that contain complementary sequences of mRNA to be imaged. The approach on the right images transgenes (transplanted genes) administered to the subject. The PET reporter gene (PRG) and therapy gene with common promoter are administered to the subject through a vehicle such as a virus. Virus transfers PRG and therapy gene to cells of the subject. Radiolabeled PET reporter probe (PRP) is then intravenously injected to determine whether gene expression is occurring from PRG.

**EXAMPLE 4-7**

Does imaging of endogenous gene expression satisfy the molecular probe requirements outlined above (under Molecular Probe Design: General Principles, p. 272)?

**ANSWER**

Let's analyze the major requirements:

1. Target specificity by the RASON is achieved by the pairing process (A-U and C-G) described above. mRNA is typically several hundred to several thousand nucleotide units, but only limited portions of the sequence are exposed for pairing to the radiolabeled probe because of the secondary and tertiary structures of the mRNA. It has been established that only 11 to 15 bases are necessary in the RASON for selective pairing of all mRNA expressed from the human genome[38] (Figure 4-9). The binding affinity of antisense molecules for mRNA is very

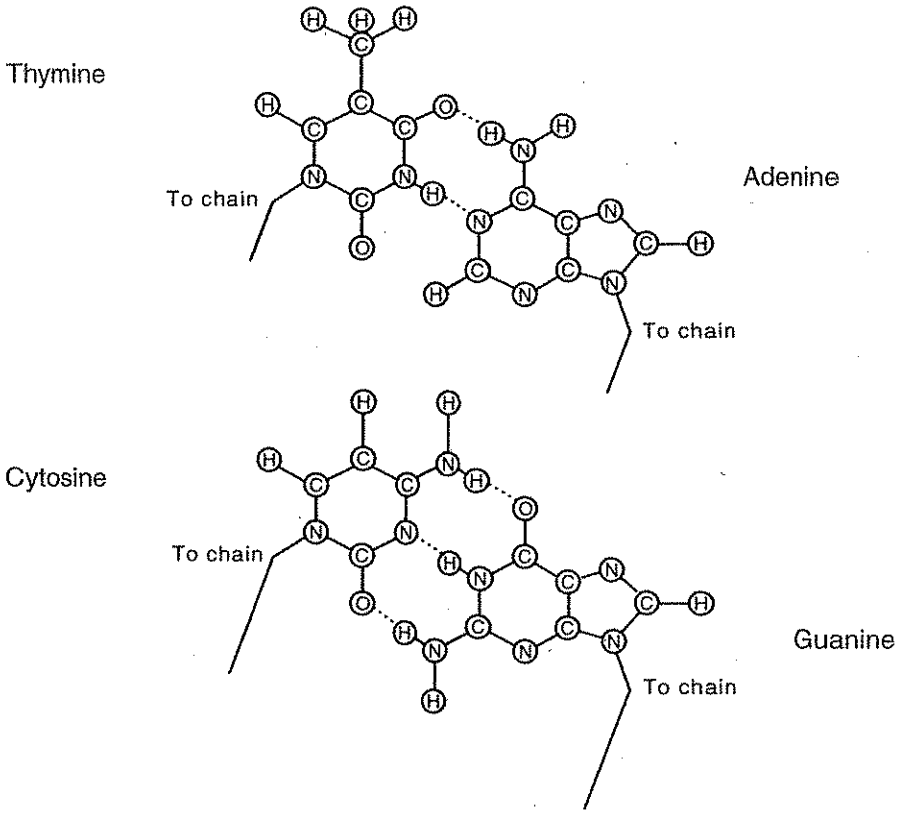


**FIGURE 4-10.** Hydrogen-bonded base pairs adenine-thymine and guanine-cytosine, the four common bases found in DNA.

high, but it can drop significantly, as much as 300-fold, with a single mismatch (e.g., when a U pairing with A is replaced by C, G, or A).[41] The pairing specificity and the strength of binding will ensure RASON trapping in a slow turnover pool upon binding to mRNA.

2. The stoichiometric basis of the binding to the target mRNA molecule imposes strict requirements of specific activity for RASON. Normal mRNA concentrations are 1 to 1,000 pmol/L, although in disease (i.e., cancer) mRNA can be expressed 100 to 10,000 times higher.[36,37,42] It has been estimated[42] that the lower limit of 1 pmol/L for mRNA concentrations will require RASON specific activities of 1 to 10 Ci/$\mu$mol that can be easily achievable with F-18 labeling.
3. Membrane permeability for RASON to access mRNA targets may be a limiting factor. Oligonucleotides are charged molecules that cross membranes using various transport mechanisms including receptor-mediated endocytosis, adsorptive endocytosis, and pinocytosis, but the rates of these processes are not well known. Clearly, oligonucleotides cannot cross the blood-brain-barrier, but delivery of RASON to the brain can be achieved using a brain drug targeting technology.[43] The ratio of specific binding to nonspecific bind-

ing occurring within cells as a function of time is related to the concentration of the target mRNA, to the concentration of nonspecific sites, and to the rate of back transport of RASON, but this will be less of a drawback with high mRNA expression.[43]

4. Peripheral metabolism should also be carefully considered when using RASON for imaging gene expression. Different structural variations of antisense imaging probes can be used: 3',5'-phosphodiester oligonucleotides (PO-ODN); 3',5'-phosphorothioate PS-ODN; and ODNs with a peptide backbone (PNA). PO-ODNs are rapidly degraded by endo- and exonucleases that break down the oligonucleotide throughout the body. This can severely limit their utility *in vivo*. 2'-Substituted PO-ODNs are better candidates because of their increased resistance to nuclease hydrolysis. PS-ODNs are not good substrates for nucleases, which dramatically increase their metabolic stability *in vivo*. However, their *in vivo* use has definite drawbacks resulting from high PS-ODN affinity for cellular and plasma proteins potentially resulting in high, nonspecific binding and reduced signal-to-noise. PNAs, having a peptide backbone, are completely stable to nucleases. However, they do not cross cell membranes well. RASON delivery technologies[45] and specific 2'-ODN modifications are being developed to overcome the important issues of membrane permeability and peripheral metabolism. This is an active area of research for imaging probes as well as drugs that are being developed to block translation of disease-mediating mRNAs into proteins.

### *Targeting enzymes without catalytic transformation of the molecular imaging probe*

This chapter reviewed that tissue enzymes can be targeted with radiolabeled substrates and analogs for *in vivo* assessment of their functionality. This approach has been most successfully used with the application of the concept of metabolic trapping [see Using Substrate Analogs of Enzyme Function (p. 282); Figure 4-3]. However, enzyme localization and function can also be assessed with molecular imaging probes that bind to enzymes, either covalently or noncovalently in a process similar to the one described for receptor-ligand interactions (Figure 4-8). The most successful and elegant studies with PET were performed with C-11-labeled compounds (e.g., chlorgyline (N-[3-(2,4-dichlorophenoxy)propyl-N-methyl-2-propynylamine) and L-deprenyl [(−)-N, $\alpha$-dimethyl-N-2-propynyl-phenethylamine] that irreversibly bind to monoamine oxidase (MAO) A and B, respectively.[44] The covalent binding to the enzyme itself by clorgyline and L-deprenyl follows the principle frequently referred to as suicide enzyme inactivation.[45] The use of these radiolabeled molecular imaging probes with PET in humans was based on the original development and use of these MAO inhibitors as drugs. Because probes based on the principle of suicide enzyme inactivation selectively bind to the target enzyme only when active, they provide a means to assay the amount of enzyme in the functional state. PET studies with these suicide enzyme inactivation probes have allowed: 1) determination of the *in vivo* distribution of MAO A and B in the human brain, 2) understanding of the effect of antidepressant drugs and smoking on brain MAO activities, and 3) assessment of the rate of recovery of MAO activities in the human brain.

## Probes targeting pathological deposition

When the tissue target is not an enzyme or receptor system, either endogenous or purposely introduced (see below, this chapter, *In vivo* Imaging of Transgenic Gene Expression, p. 298) but rather a protein or other tissue target resulting from the specific pathology, imaging probes can be designed to target them. The best known example is the targeting of radiolabeled antibodies to sites on the surface of tumor cells. This is discussed in Chapter 2 with the use of engineered minibodies and antibodies. Other examples of these imaging probes are now emerging together with a more complete understanding of the specific pathologies. One such example is the development of molecular imaging probes to target β-amyloid plaques and neurofibrillary tangles in the brain of patients with Alzheimer's disease. Common features in the brain of patients with familial or sporadic Alzheimer's disease include the presence of abundant intraneuronal neurofibrils (NFTs), extracellular amyloid rich β-amyloid plaques (APs), and neuronal loss.[46] The difficulty in finding such molecular imaging probes to target these pathologies resides mostly in the fact that most probes known to bind amyloid plaques (i.e., Congo red, chrysamine G) do not appreciably cross the blood-brain-barrier, making them essentially useless *in vivo*. A new generation of radiolabeled, highly hydrophobic naphthalene derivatives has been developed and used in humans.[47,48] These compounds have the ability to easily diffuse into the brain and bind to both β-amyloid plaques and neurofibrillary tangles with various degrees of specificity. Results were confirmed by brain autoradiography in the same brain specimens matching results with immunostaining (Figure 4-11).[49] Because these probes are fluorescent, binding is also demonstrated with confocal fluorescent microscopy and *in vitro* binding affinity measurements with β-amyloid neurofibrils. Moreover, the binding of several nonsteroidal anti-inflammatory drugs (NSAIDs; e.g., naproxen, ibuprofen) to the same β-amyloid site was demonstrated by competitive kinetics with the radiolabeled naphthalene probes[50] (see Molecular Imaging and Drug Development, p. 310).

**EXAMPLE 4-8**

Are amyloid molecular imaging probes analogous to receptor binding probes in their mode of binding?

**ANSWER**

In a way, they are. β-amyloid peptides aggregate by forming extended chains of cross β sheets, which, in turn, form tubular, 30Å-diameter protofilaments, with three to five of these protofilaments constituting the amyloid fibril. Multiple fibril aggregates form amyloid plaques. Therefore, the amyloid fibril is organized as a tubular micelle with polar domains forming the outer wall of the amyloid fibril while the hydrophobic domain is at the center of the fiber (Figure 4-12). Thus, APs have multiple binding sites as evidenced by the presence of at least two kinetically distinguishable binding affinities with these probes.[50]

## Drug mimicking imaging probes

There are few examples in PET that better illustrate the marriage of therapy (drug interventions and treatment) and diagnostics using molecular imaging than en-

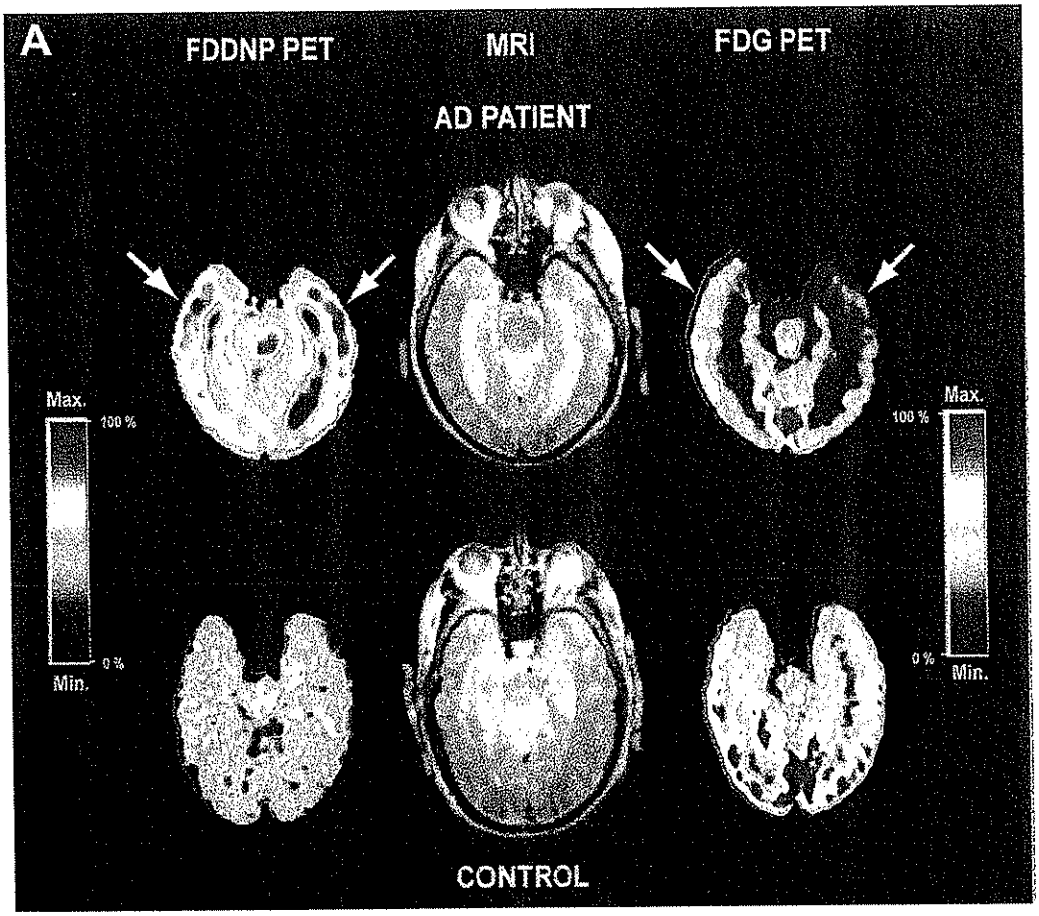
A
FDDNP PET
MRI
FDG PET
AD PATIENT
Max.
100 %
0 %
Min.
Max.
100 %
0 %
Min.
CONTROL

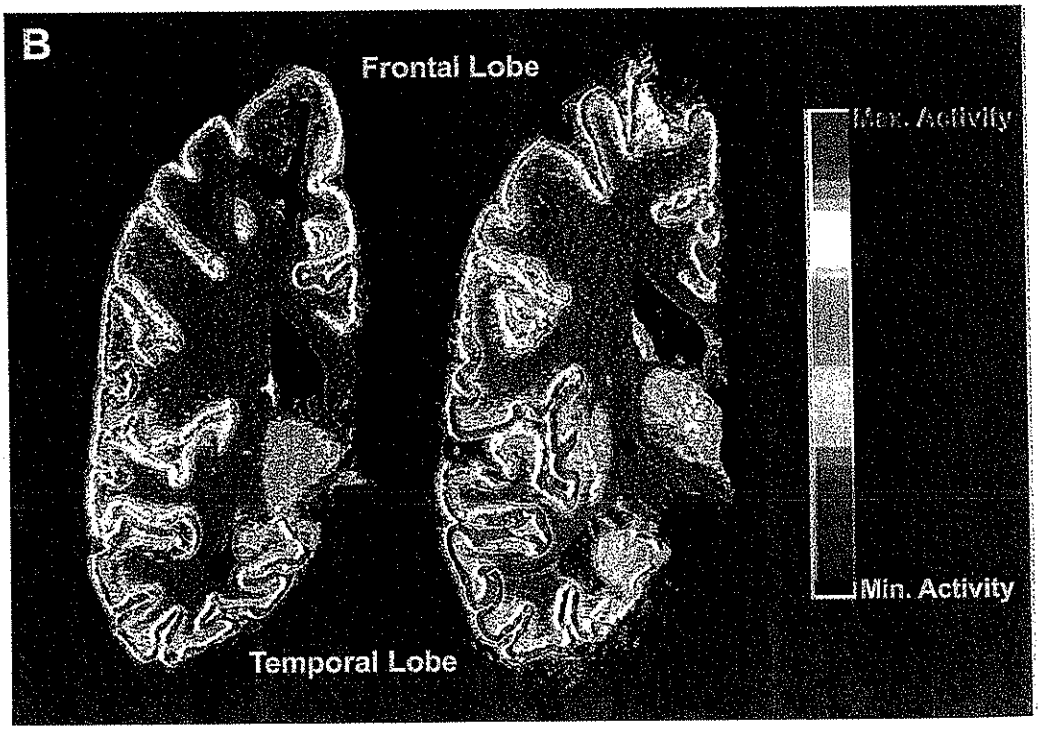
B
Frontal Lobe
Max. Activity
Min. Activity
Temporal Lobe

**FIGURE 4-11.** A direct comparison of *in-vivo* PET (A) and *in-vitro* digital autoradiography (B) for detection of β-amyloid senile plaques (SPs) and neurofibrillary tangles (NFTs) in the brain of a patient with Alzheimer's disease (AD). PET and autoradiography utilized the molecular imaging probe, 2-(1-{6-[2-[F-18]fluoroethyl)(methyl) amino]-2-naphthyl}ethylidene)malononitrile (-18]FDDNP). Subset A shows the FDDNP and FDG–PET images coregistered to their respective MRI images. Areas of FDG hypometabolism are matched with the localization of NFTs and APs resulting from FDDNP binding (marked arrows). The [$^{18}$F]FDDNP images were obtained by summing frames 12 to 14, corresponding to 25 minutes to 54 minutes post-FDDNP administration. The FDG images were obtained by summing frames corresponding to 20 minutes to 60 minutes postFDG injection. The color bar represents the scaling of the FDDNP and FDG images. (Reprinted from Shoghi-Jadid et al,[48] with permission from the American Psychiatric Association.) Subset B demonstrates the power of autoradiography to map localization of NFTs and APs in brain specimens from patients with Alzheimer's disease.

dogenous gene expression with ODNs (see above) and transgenic expression determinations. For example, human gene therapy trials with exogenous genes (transgenes) can be significantly aided by the ability to locate, determine the magnitude of, and establish time-dependent changes in gene expression. Assay techniques are described in Chapter 2.

**FIGURE 4-12.** Schematic representation of β-amyloid plaque formation in brain tissue, a phenomenon associated with Alzheimer's disease. Because of their ambiphilic nature, amyloid peptides aggregate, forming simple microtubules that associate to form neurofibrils with multiple microtubules. Neurofibril aggregates form neurofibrillary plaques that frequently have cellular debris.

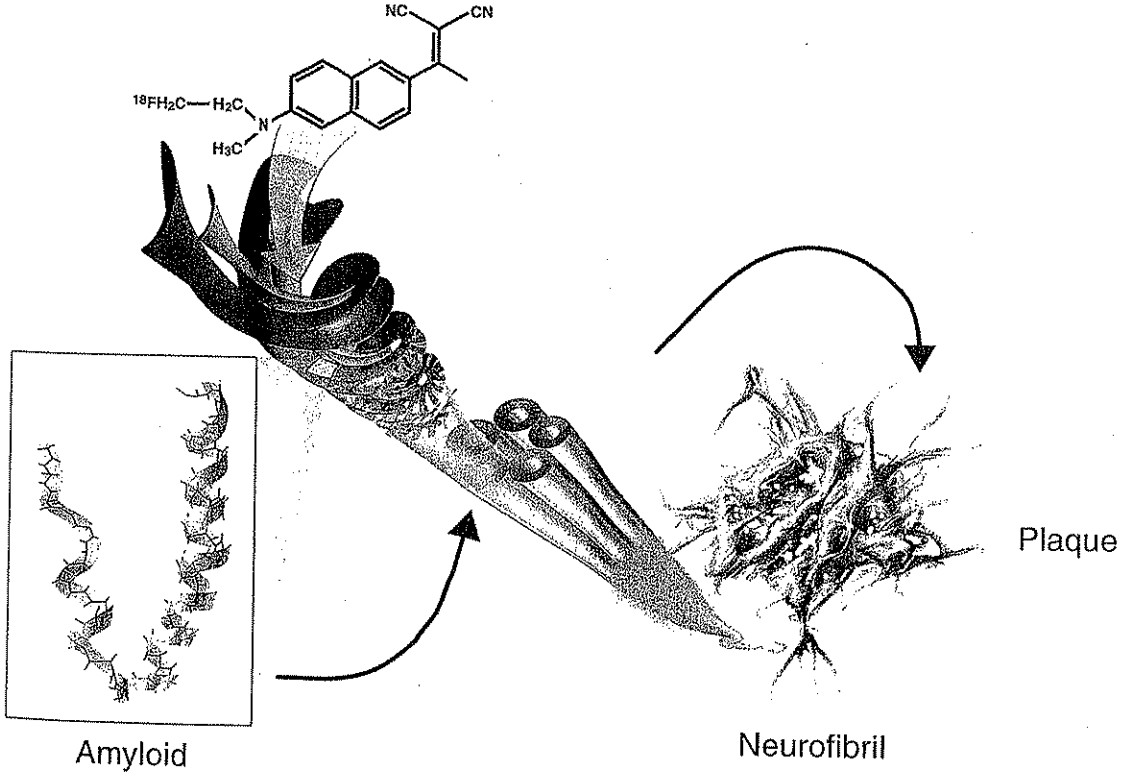

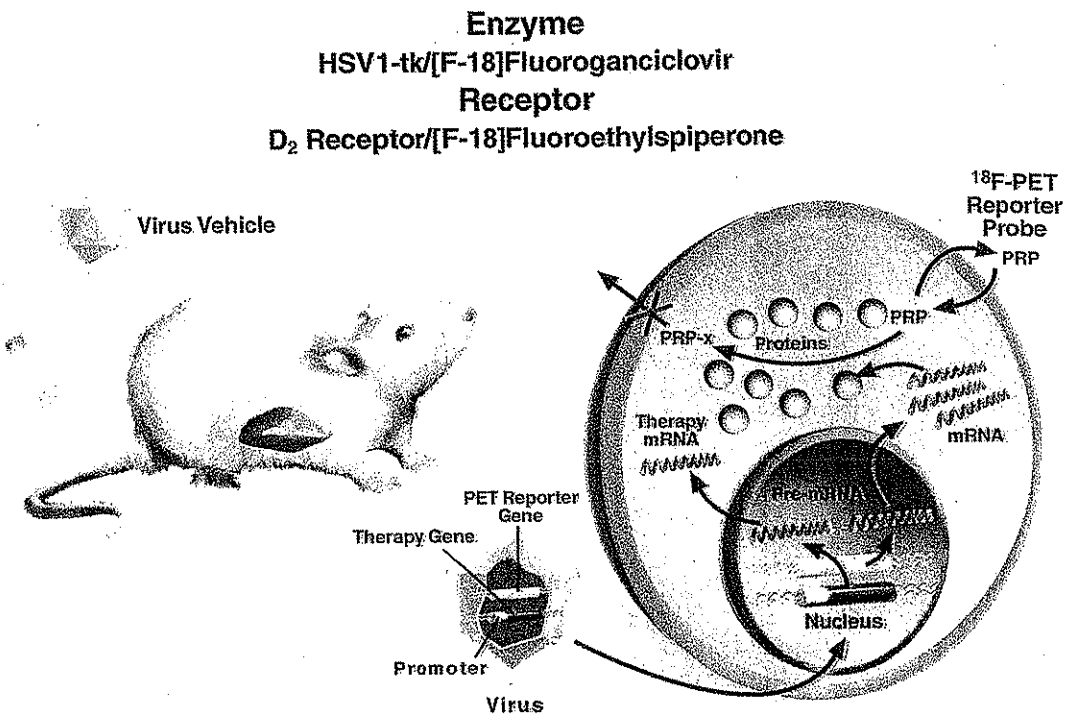


**FIGURE 4-13.** PET reporter gene-PET reporter probe (PRG–PRP) approach using either enzyme or receptor gene as PRG system. In this example, PRG reporter and therapy gene are placed in virus, which is injected into the tail vein of a mouse. Virus is delivered throughout the body via the bloodstream and localizes in the liver. Virus then transfers PRG and therapy gene to cells in the liver. Because of a common promoter, the expression of PRG corresponds to the expression of therapy gene. The PRG and therapy gene can also be connected together via a common promoter in a single construct (Chapter 2). PRG expression proceeds through transcription to mRNA and then translation to the protein product. In an enzyme example with herpes simplex virus thymidine kinase (HSV-1-tk) gene, the protein product is HSV-1-TK enzyme. The mouse then receives an intravenous injection with the PRP, [F-18]fluoroganciclovir, which diffuses into cells and is cleared to the bladder. If gene expression is present, HSV-1-TK enzyme phosphorylates [F-18]fluoroganciclovir, which is retained in the cell. In the receptor approach, [F-18]fluoroethylspiperone is used as PRP to bind to the $D_2$ receptor, which is the protein product of PRG.

### In vivo *imaging of transgenic expression with herpes simplex virus thymidylate kinase (HSV1-TK): focus on probe-binding interactions*

Molecular imaging probes for HSV1-TK were developed on the same principles that produce metabolic trapping of the product of the HSV1-TK reaction, as phosphorylated substrate in a process similar to the phosphorylation of FDG by hexokinase (Figure 4-13). In terms of probe design, ideal reporter probes for HSV1-TK, the enzyme product of the reporter gene HSV1-tk, should be good substrates for the enzyme and poor substrates for mammalian TK (mTK), an endogenous cytosolic enzyme [e.g., kcat (or Vm)/Km for HSV1-TK $\gg$ kcat (or Vm)/Km for mTK]. It should also be understood that the imaging probe will have to compete *in vivo* with endogenous thymidine, a substrate with very favorable kinetics for HSV1-TK.[36]

To date, two main substrate groups have been developed as reporter probes for HSV1-TK: 1) pyrimidine analogs and 2) acycloguanosine derivatives (Figure 4-14; Table 4-5).[38,39,51–104] Pyrimidine analogs [e.g., 5-iodo-2′-fluoro-2′-deoxy-1-β-D-arabinofuranosyl-5-iodouracil (FIAU) radiolabeled with C-14, I-131 or I-124] have very high sensitivity as imaging agents because they are high affinity substrates for HSV1-TK. Their Vm and Km approach those of the endogenous substrate thymidine.[36] However, they are also excellent substrates of the endogenous mammalian TK, thus reducing their specificity for the HSV1-TK infected-target tissue. Some differences do exist, however, between the in vivo kinetics of the interaction of FIAU with HSV1-TK and mammalian-TK because some imaging specificity is obtained when clearance of the nontarget component of the label is allowed. For example,

**FIGURE 4-14.** Structures of thymidine, guanosine, and closely related analogs with affinity for HSV1-TK. Radiolabeled versions of these molecules produced molecular imaging probes used in the assessment of HSV1-tk mediated gene expression *in vivo* with PET.

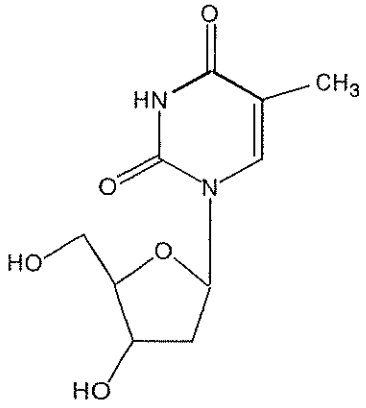


Thymidine

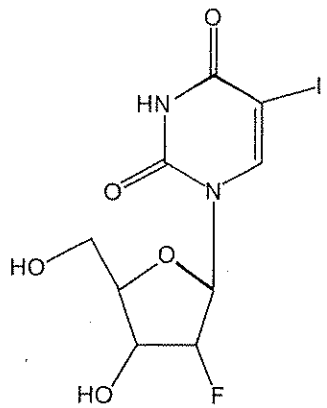


FIAU

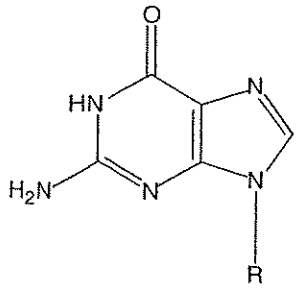


R

| Deoxyribose | Deoxyguanosine |
|---|---|
| 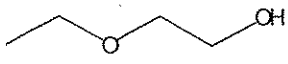 | Acyclovir |
| 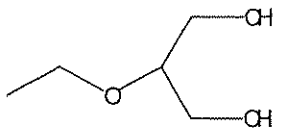 | Ganciclovir |
| 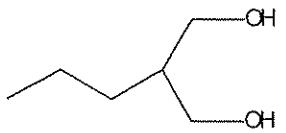 | Penciclovir |

**TABLE 4-5. Summary of Reporter Gene/probe Systems**

| *Reporter gene* | *Mechanism* | *Imaging agents* | *Imaging* | *References* |
|---|---|---|---|---|
| Cytosine deaminase | Deamination | [$^{3}$H]-5-fluorocytosine | Cell culture study | Haberkorn et al. (1996)[52]<br>Stegman et al. (1993)[53] |
| | | [$^{19}$F]-5 fluorocytosine | MRS | |
| Herpes-simplex virus type 1 thymidine kinase (HSV1-tk) | Phosphorylation | [$^{131}$I]FIAU, [$^{14}$C]FIAU | SPECT, gamma camera | Tjuvajev et al. (1996)[54] |
| | | [$^{131}$I]FIAU | SPECT, gamma camera | Tjuvajev et al. (1999)[55] |
| | | [$^{124}$K]FIAU | PET | Tjuvajev et al. (1999)[56] |
| | | [$^{123/125}$]FIAU | Gamma camera | Haubner et al. (2002)[57] |
| | | [$^{125}$]IVDU, [$^{125}$I]IVFRU, [$^{125}$I]VFAU, [$^{125}$I]IVAU | Cell culture | Morin et al. (1997)[58] |
| | | [$^{125}$I]FIAU, [$^{125}$I]FIRU | Cell culture | Wiebe et al. (1999)[59] |
| | | [$^{3}$H]FFUdR | Cell culture | Germann et al. (1998)[60] |
| | | [$^{14}$C]GCV, [$^{3}$H]GCV | Autoradiography | Gambhir et al. (1998)[61]<br>Haberkorn et al. (1997)[62]<br>Haberkorn et al. (1998)[63] |
| | | [$^{18}$F]GCV | PET | Gambhir et al. (1999)[37]<br>Gambhir et al. (1998)[61] |
| | | [$^{18}$F]PCV | PET | Iyer et al. (2001)[64] |
| | | [$^{18}$F]FHPG | PET | Alauddin et al. (1996)[65]<br>Alauddin et al. (1999)[66]<br>de Vries et al. (2000)[67]<br>Hospers et al. (2000)[68]<br>Hustinx et al. (2001)[69] |
| | | [$^{18}$F]FHBG | PET | Alauddin and Conti (1998)[70]<br>Yaghoubi et al. (2001)[71] |
| Mutant Herpes-simplex virus type 1 thymidine kinase (HSV1-sr39-tk) | Phosphorylation | [$^{18}$F]PCV | Cell culture, PET | Gambhir et al. (2000)[38]<br>Sun et al. (2001)[72] |
| | | [$^{18}$F]FHBG | | Yaghoubi et al. (2001)[71]<br>Yu et al. (2000)[39] |
| Dopamine2 receptor | Receptor-ligand | [$^{18}$F] FESP | PET | MacLaren et al. (1999)[73]<br>Sun et al. (2001)[72]<br>Yaghoubi et al. (2001)[74]<br>Yu et al. (2000)[39] |
| Mutant Dopamine2 receptor | Receptor-ligand | [$^{18}$F] FESP | PET | Liang, et al. (2001)[75] |
| Somatostatin receptor | Affinity binding | [$^{111}$In]DTPA-D-Phe$^{1}$-octreotide | Gamma camera | Rogers et al. (1999)[76] |
| | | [$^{64}$Cu]-TETA-octreotide | Tumor uptake study | Buchsbaum et al. (1999)[77] |
| | | [$^{188}$Re]-somatostatin analogue, $^{99m}$Tc somatostatin analogue | Gamma camera | Rogers et al. (2000)[78]<br>Zinn et al. (2000)[79] |

**TABLE 4-5. (continued)**

| *Reporter gene* | *Mechanism* | *Imaging agents* | *Imaging* | *References* |
|---|---|---|---|---|
| Oxotechnetate-binding fusion proteins | Binding via transchelation | [$^{99m}$Tc] Oxotechnetate | Autoradiography<br>Gamma camera | Bogdanov et al. (1997)[80]<br>Bogdanov et al. (1998)[81] |
| Gastrin-releasing peptide receptor | Affinity binding | [$^{125}$I]-mIP-Des-Met$^{14}$-bombesin (7-13)$NH_2$ | Cell culture | Baidoo et al. (1998)[82]<br>Rogers et al. (1997)[83] |
| | | [$^{125}$I]bombesin, | Cell culture | Rogers et al. (1997)[84]<br>Rosenfeld et al. (1997)[85] |
| | | [$^{99m}$Tc]-bombesin analogue | Cell culture | |
| Sodium/iodine symporter (NIS) | Active symport | [$^{131}$I] | Gamma camera | Boland et al. (2000)[86]<br>Haberkorn et al. (2001)[87] |
| Tyrosinase | Metal binding to melanin | Synthetic metallomelanins [$^{111}$In], Fe | Cell culture/ MRI | Enochs et al. (1997)[88]<br>Weissleder et al. (1997)[89] |
| Green fluorescent protein (GFP) | GFP gene expression resulting in fluorescence | Fluorescence | Fluorescence microscopy | Hasegawa et al. (2000)[90]<br>Pfeifer et al. (2001)[91]<br>Yang et al. (2000)[92]<br>Yang et al. (2001)[93]<br>Yang et al. (2000)[94]<br>Yang et al. (1998)[95]<br>Yang et al. (1999)[96] |
| Luciferase (firefly) | Luciferase–luciferin reaction in presence of oxygen, $Mg^{2+}$ and ATP | Bioluminescence | CCD camera | Contag et al. (1997)[97]<br>Contag et al. (1998)[98] |
| Luciferase (renilla) | Luciferase–luciferin reaction in presence of oxygen, no other cofactors required | Bioluminescence | CCD camera | Bhaumik and Ghambir (2001)[99] |
| Cathepsin D | Quenched NIRF fluorochromes | Fluorescence activation | CCD camera | Tung et al. (1999)[100]<br>Tung et al. (2000)[101] |
| $\beta$-galactosidase | Hydrolysis of $\beta$-glycoside bond | (1-(2-($\beta$-galactopyranosyloxy) propyl)-4,7,10-tris (carboxymethyl)1,4,7,10 tetraazacyclododecane) gadolinium(III) or EgadMe | MRI | Weissleder et al. (1999)[102]<br>Louie et al. (2000)[103] |
| Engineered transferrin receptor (TfR) | Receptor-ligand, internalization | Superparamagnetic iron | MRI | Weissleder et al. (2000)[104] |

*Abbreviations*: ATP, adenosine triphosphate; CCD, charged coupled device; MRI, magnetic resonance imaging; MRS, magnetic resonance spectroscopy; NIRF, near-infrared fluorescent probes; PET, positron emission tomography; SPECT, single photon emission computed tomography.

*Source*: Adapted from Ray et al,[51] with permission from Elsevier.

[I-124]FIAU has been successfully used with PET in animals with implanted tumors with various levels of HSV1-TK expression, but many hours (e.g., 30) were necessary to achieve the required specificity, namely, high ratios of specific (i.e., produced by the HSV1-TK-mediated phosphorylated product of [$^{124}$I]FIAU) to nonspecific background activity.[54] Molecular probes have also been developed and used with other gene reporter systems (Table 4-5).[38,39,51–104]

Acycloguanosine derivatives have also been extensively investigated as PET reporter probes for HSV1-TK. A detailed description of their utilization in mice models using microPET technology is presented in Chapter 2. This chapter outlines the principles of their utilization based on their kinetic properties with HSV1-TK.

Using acycloguanosine derivatives as PET reporter probes with the HSV1-tk PET reporter gene is based on the utilization of acycloguanosines (most notably, acyclovir and ganciclovir) as therapeutic agents for herpes simplex virus infections and in gene therapy protocols, using the HSV1-TK/ganciclovir suicide system to treat many forms of cancers[105–107] and AIDS.[108,109]

9-[2-Hydroxyethoxymethyl]guanine (acyclovir) was shown 25 years ago to be specifically phosphorylated by HSV1-TK. This discovery constituted the basis of the successful treatment of Herpes simplex virus infection. Since then, other acycloguanosines (Figure 4-14) have been developed with even better efficacy as therapeutic agents. In all cases, the phosphorylated acycloguanosine derivatives are converted by cellular enzymes to their corresponding triphosphates which, upon incorporation into the viral DNA, produce chain termination and thereby interrupt the vital cycle of virus replication. The safety of acycloguanosines as therapeutic agents is predicated on the premise that they are poor substrates for mammalian TK. Therefore, phosphorylation only occurs in virus-infected cells, which minimizes toxic effects. The low affinity of acycloguanosines for mammalian TK and high affinity for HSV1-TK is also a very important property for utilization of these acycloguanosines as PET reporter probes to produce high specificity in the image.

There are no amino acid sequence similarities between HSV1-TK and mammalian TK.[110] However, both enzymes may share their ability to bind the natural substrate, thymidine, and some pyrimidine analogs very efficiently. HSV1-TK also phosphorylates purine as well as pyrimidine analogs. It also has low specificity for the ribosyl moiety in nucleoside, readily accepting cyclic and acyclic side chains. Therefore, the different characteristics of the binding sites of both enzymes permit exploitation of this feature in the design of radiolabeled acycloguanosine analogs as molecular imaging probes.

First, it is important to understand the binding characteristics of thymidine to HSV1-TK. The reported Km of thymidine for HSV1-TK is in the range 0.2 $\mu$m to 8.5 $\mu$M (most likely, submicromolar is the most accurate value) whereas thymidine plasma concentration is 0.05 $\mu$M to 0.5 $\mu$M. This presents thymidine as a formidable competitor for HSV1-TK sites *in vivo*, which necessitates imaging probes with high affinity and catalytic efficiency (high kcat/Km) for high signal-to-noise ratios in the tomographic images (see above). A map of the HSV1-TK active site obtained with X-ray crystallography (Figure 4-15) shows the binding characteristics of thymidine to HSV1-TK. Interaction of the pyrimidine ring is via its C-4 carbonyl and 3-NH group with the amide group of glutamine-

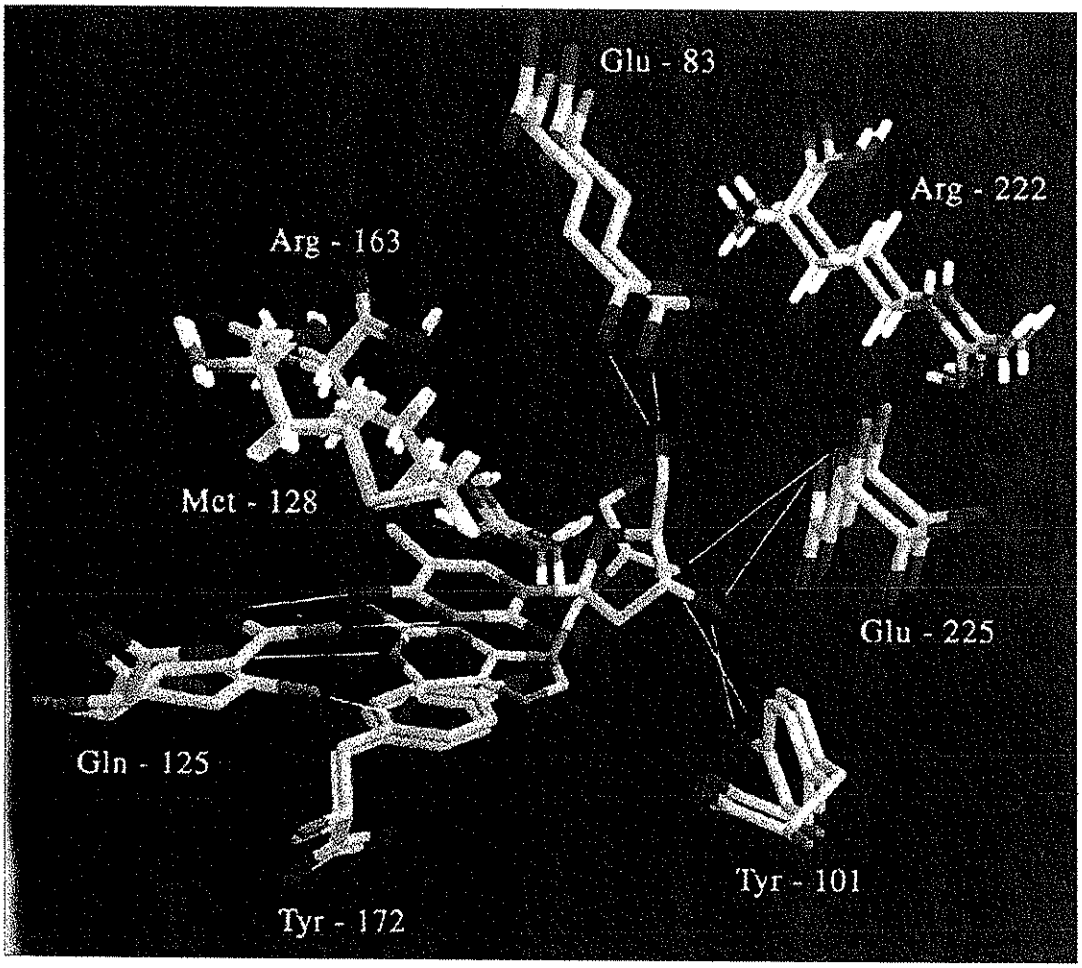


**FIGURE 4-15.** Binding modes of thymidine (dark gray bonds) and ganciclovir (light gray bonds) in the active site pocket of HSV-1-TK. Oxygen and nitrogen atoms are drawn as light and dark gray spheres, respectively. Hydrogen bonds are indicated as dashed lines. There is a remarkable overlap between amino acid side chains in the two active-site pockets. The only exception is glutamine-125, whose amide functionality is flipped approximately 180 between the two crystal forms in order to optimize hydrogen-bonding opportunities. See ref. 111 and 112

125 and arginine-176, via two water molecules. Also, the pyrimidine ring is sandwiched and fixed between methionine-128 and tyrosine-172. The 3′-OH in the deoxyribose moiety binds with tyrosine-101 and glutamate-225 and the 5′-OH with glutamate-83. The site also has a domain (LID domain) that closes[111] and is expected to undergo conformational changes upon substrate and ATP binding for phosphoryl-transfer.

Binary complexes of acycloguanosines (i.e., acyclovir, ganciclovir, and penciclovir) with HSV1-TK were also determined by X-ray crystallography at 2.37 Å resolution (Figure 4-15). The guanine base occupies approximately the same geometric plane as the pyrimidine (in thymidine). Similarly, the guanine NH-1

and 6-carbonyl groups form hydrogen bond pairing with glutamine-125 and arginine-176. The hydrogen bond with glutamine-125 involves a conformational shift of the side chain as well as a 180° rotation of the amide. There are only slight variations in the hydrogen-bonding pattern of the guanine moiety among these acycloguanosine analogs. The acycloriboside moiety (in acycloguanosines) and the deoxyribose (in thymidine) are similarly located at the binding site. The single hydroxyl of acyclovir [and the pro-(S)-groups of ganciclovir and penciclovir] mimics the 5′-OH interactions of ribose.[112]

The introduction of radiolabeled fluorine to acycloguanosines[70,113,114] produces structural features that modify their binding parameters (Km, kcat) as well as their catalytic efficiency (kcat/Km) and, as a result, their ability to act as molecular imaging probes (Table 4-6). A combination of two factors decreases substrate specificity for HSV1-TK: 1) Carbon-8 fluorine substitution destabilizes guanine binding by modifying aromatic ring stacking with tyrosine-172 and hydrogen bonding with glutamine-125 and arginine-176, and 2) the simultaneous presence of C-8 fluorine/C-2′-oxygen induces a shift from anti- to a preferred quasi-syn conformation, redirecting the 5′-OH (the phosphoryl acceptor) away from the ATP binding domain. When the fluorine is in the lateral chain, in both ganciclovir and penciclovir, guanine binding characteristics are preserved, and as a result, these compounds present the highest catalytic efficiency (particularly the fluorinated penciclovir analog, FHBG (Tables 4-5[38,39,51–104] and 4-6). These properties are matched by the ability of these radiofluorinated analogs to act as *in vivo* molecular imaging probes (see Chapter 2).

Moreover, the availability of HSV1-TK mutants (e.g., HSV1-sr39TK) with increased efficiency for acycloguanosines and decreased efficiency for endogenous thymidine makes this reporter gene/PET reporter probe system even more attractive for *in-vivo* gene expression determinations.[115]

### *Probing the functional integrity of neurotransmitter systems*

The significance of the dopaminergic system in health and disease states, such as its well determined role in neurodegenerative disorders involving motor function (e.g., Parkinson's disease), emotional disorders (e.g., schizophrenia), and the effects of drugs of abuse (e.g., cocaine and m-amphetamine), has made it the best studied central neurotransmitter system *in vivo*. A plethora of molecular imaging probes have been developed in the last 20 years to evaluate the functional integrity of the dopaminergic system, involving probes of enzyme function acting as substrates (e.g., FDOPA, 4- and 6-[F-18]fluoro-L-m-tyrosine) or binding stoichioimetrically to enzymes (i.e., C-11 deprenyl), probes of the presynaptic dopamine reuptake carrier (e.g., WIN analogs, ritalin, and cocaine), and postsynaptic receptor probes (e.g., dopamine D1, D2, D3, and D4 probes) (Figure 4-16). The dopaminergic system is used in this chapter as an example of how multiple probes have been constructed to dissect the various biochemical components of a neurotransmitter-based cell communication. Reviews of molecular imaging probes for other neurotransmitter systems can be found elsewhere.[116]

Among molecular imaging probes of enzyme function, FDOPA has been exhaustively studied from a mechanistic perspective.[117] FDOPA has already demonstrated its value as a diagnostic tool for movement disorders and its utilization resulted in major discoveries in the neurodegenerative process leading

**TABLE 4-6. The Efficiency of Radiolabeled Fluorine Bound to Acycloguanosines to Serve as Molecular Imaging Probes**

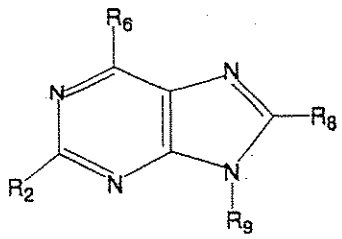


| *Compound name* | *Compound number* | *R-2* | *R-6* | *R-9* | *R-8* | *Km (μM)* | *kcat (s-1)* | *Kcat/Km (s-1 M-1)* | *λmax (nm)* | *E (10-3 M/cm)* | *Relative imaging efficiency (in vivo) using PET and F-18-labeled substrate* |
|---|---|---|---|---|---|---|---|---|---|---|---|
| Acyclovir | 1 | —NH2 | —OH |  | —H | 3.87 | 0.08 | 20763 | 250 | 13.53 | NA |
| 8-Fluoroacyclovir | 2 | — | — | | —F | 221.14 | 0.11 | 513 | 240 | 4.82 | + |
| Ganciclovir | 3 | — | — | 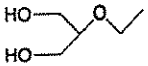 | —H | 10.23 | 0.26 | 25649 | 250 | 14.30 | NA |
| 8-Fluorogancyclovir | 4 | — | — | | —F | 396.39 | 0.4 | 1004 | 242 | 3.91 | ++ |
| Penciclovir | 6 | — | — | 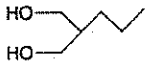 | —H | 3.55 | 0.04 | 11745 | 252 | 11.97 | NA |
| 8-Fluoropenciclovir | 7 | — | — | | —F | 11.63 | 0.07 | 6452 | 242 | 3.23 | +++ |
| Rac-side-chain-fluoroganciclovir | 5 | — | — | 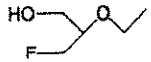 | —H | 2.23 | 0.07 | 33290 | 250 | 13.98 | ++++ |
| Rac-side-chain-fluoropenciclovir | 8 | — | — | 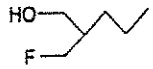 | —H | 0.94 | 0.04 | 45428 | 250 | 11.84 | +++++ |

*All compounds dissolved in 50 mM Tris-HCl buffer, pH 7.45. E($10^{-3}$ M/cm) for guanosine ($\lambda_{max}$: 252 nm) = 13.20

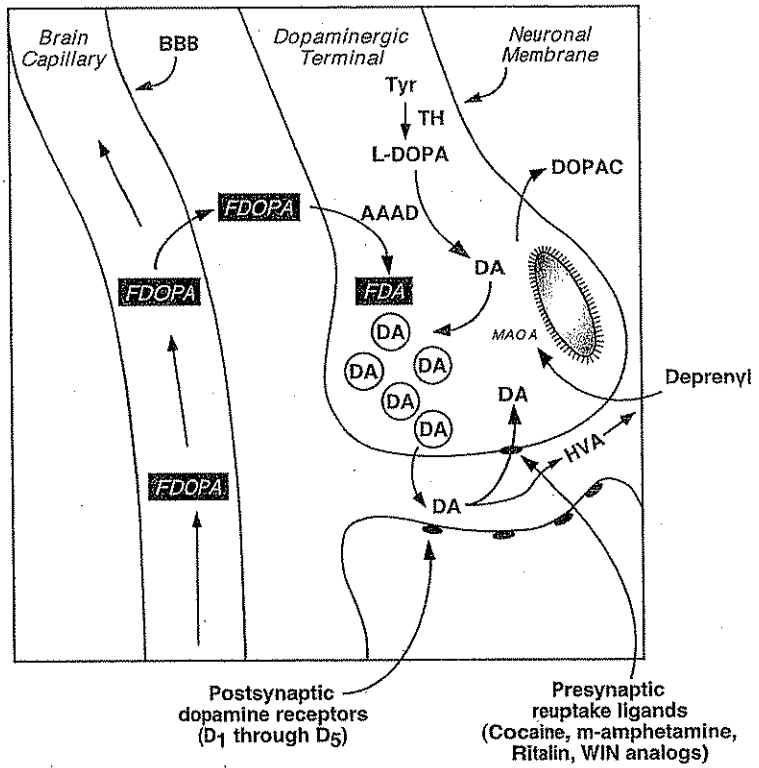


**FIGURE 4-16.** Schematic representation of a cellular dopaminergic terminal. The use of molecular imaging probes with PET for presynaptic function assessment (e.g., FDOPA) or presynaptic dopamine reuptake ligands (e.g., cocaine) or postsynaptic function (e.g., dopamine $D_1$-$D_5$ receptors) permits the biochemical dissection of the system. Abbreviations: AAAD, aromatic L-amino acid decarboxylase; BBB, blood-brain-barrier; DA, dopamine; DOPAC, dihydroxyphenylacetic acid; FDOPA, L-3,4-dihydroxy-6-[18F]fluoro-phenyl-alanine; HVA, homovanillic acid; L-DOPA, levodopa; MAO A, monoamine oxidase A; TH, tyrosine hydroxylase; Tyr, tyrosine.

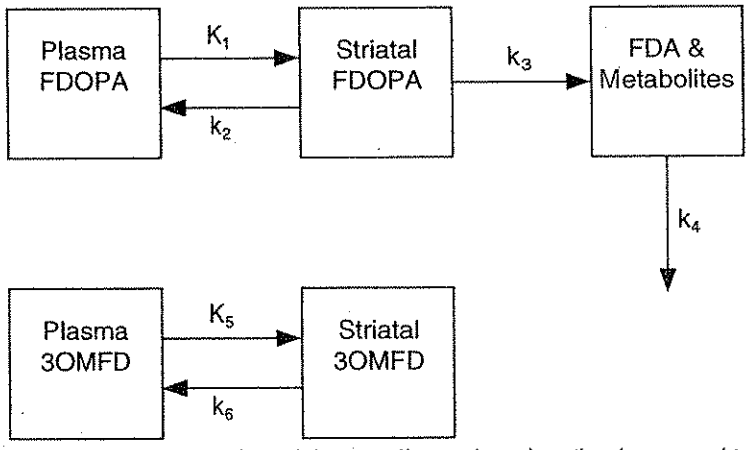


**FIGURE 4-17.** Compartmental model generally used to describe the tracer kinetics of 6-[$^{18}$F]fluoro-L-DOPA (FDOPA) in brain tissue.

to Parkinson's disease progression (Chapter 7). As an analog of L-DOPA, FDOPA is decarboxylated by aromatic-L-aminoacid decarboxylase (AAAD) to 6-[F-18]fluorodopamine (FDA) that, like dopamine, accumulates in vesicles in the neurotransmitter terminal. This is a slow turnover rate functional pool with a turnover rate of 0.21 $h^{-1}$.[118,119] Thus, this trapping mechanism is a variation of the metabolic trapping via phosphorylation illustrated above with FDG/hexokinase and fluoroguanosines (or FIAU)/HSV1-TK. Based on this knowledge, various methods have been used to quantify accumulation of FDA, including simple specific-to-nonspecific ratios[120] and compartmental models with various degrees of complexity. Typically, these models represent reversible competitive transport of FDOPA across the blood-brain-barrier (K1/k2); AAAD-mediated decarboxylation and trapping (k3); and FDA vesicle release, metabolism, and tissue clearance (k4). The formation of peripheral metabolites (i.e., 3-O-methyl-[F-18]fluoro-L-DOPA, 3OMFD) is also represented in the mathematical model (Figure 4-17).

For analysis of the various tracer kinetic models, estimations, and constraints, the reader is referred to the above-mentioned references and Chapter 2.

**EXAMPLE 4-9**

How does FDOPA decarboxylation rate [k3 (PET)] relate to dopamine synthesis?

**ANSWER**

Under the conditions of uniform concentration of both enzyme and substrate, the competitive conversion of FDOPA (and L-DOPA) to FDA (or dopamine) follows the Michaelis–Menten equation as described in Equation 4-27. L-DOPA and FDOPA have similar Km and Vm for AAAD (see below); therefore the lumped constant $Vm' Km/VmKm' = 1$.

As a result, Equation 4-27 can be simplified:

$$V = k'3\,(PET)[S] \qquad (4\text{-}28)$$

Thus, the value of k'3 obtained for FDOPA in the PET determination can be used to estimate the decarboxylation rate of L-DOPA *in vivo*, if the concentration of L-DOPA in tissue is known. Using the average concentration of L-DOPA in striatum of 400 nM[121] and the FDOPA rate constant k'3 of 0.02/min (Table 4-7[114,122–135]), the calculated decarboxylation rate of L-DOPA in striatum is 8 pmol/min/g.

**EXAMPLE 4-10**

Is this determination reliable? Does the L-DOPA decarboxylation rate measured *in vivo* with PET compare with values?

**ANSWER**

The PET estimations of L-DOPA utilization rates using FDOPA in humans and nonhuman primates match determinations *in vivo* in rats.[133] They also correlate with AAAD activities in dopaminergic terminals[122] but are far below the 0.3 nmol/min/g rate experimentally measured for dopamine synthesis in rodents[133] and also significantly lower than determinations *in vitro* in the same animal species.[122] Several possible explanations may account for the discrepancy between *in vivo* and *in*

**TABLE 4-7. Summary of Reported *In-Vivo* Striatal Aromatic-L-amino Acid Decarboxylase (AAAD) Rates**

| *Species* | *Assay description* | *AAAD activity [$k_3'$ (/min)]* | *Reference* |
|---|---|---|---|
| Human | FDOPA PET | 0.024 | Gjedde et al. (1991)[123] |
| Human | FDOPA PET | 0.041 | Huang et al. (1991)[124,a] |
| Human | FDOPA PET | 0.083 | Hoshi et al. (1993)[125] |
| Human | FDOPA PET | 0.021 | Ishikawa et al (1996)[126] |
| Human | FDOPA PET | 0.080 | Kuwabara et al. (1995)[127] |
| Human | FDOPA PET | 0.012 | Nahmias et al. (1996)[128] |
| Human | 6-FMT PET[a] | 0.011 | Nahmias and Wahl (1995)[129] |
| Monkey (*Macaca nemestrina*) | FDOPA PET | 0.021 | Barrio et al. (1990)[130] |
| Monkey (Vervet) | FDOPA PET | 0.015 | Barrio et al. (1996)[114] |
| Monkey (Rhesus) | L-[$\beta$-$^{11}$C]DOPA PET | 0.012 | Hartvig et al. (1993)[131] |
| Monkey (Rhesus) | L-[$\beta$-$^{11}$C]DOPA PET | 0.011 | Tsukada et al. (1996)[132] |
| Monkey (Vervet) | 6-FMT PET[a] | 0.033 | Barrio et al. (1996)[114] |
| Rat (Sprague-Dawley) | FDOPA | 0.010 | Reith et al. (1990)[133] |
| Rat (Wistar) | [$^3$H]DOPA | 0.260 | Cumming et al. (1995)[134,b] |
| Rat (Long-Evans) | FDOPA | 0.170 | Cumming et al. (1994)[135,b] |

*Source:* Reprinted with permission from Yee et al.[122]

*Abbreviations:* FDOPA, 6-[F-18]fluoro-L-DOPA; PET, positron emission tomography.

[a]6-FMT, 6-[$^{18}$F]fluoro-L-*m*-tyrosine.

[b]*Ex-vivo* experiments.

*vitro*-determined L-DOPA decarboxylation rates (Tables 4-7[114,122–135] and 4-8[122,135,137–141]). They have been summarized as follows:[122]

1. Estimated $k'_3$ values can be impacted by partial volume effects when these determinations are performed in small animals (e.g., squirrel monkeys, total brain size ~ 25 g). These effects are important when the size of the object (in this case, the object is defined by the area of interest, namely the basal ganglia) is on the same order of the spatial resolution of the PET scanner. Corrections in spill-over may increase $k'_3$ by 2- to 3-fold,[144] but they cannot account for the more than 10-fold underestimation in the $k'_3$ determination.
2. The discrepancy between *in vitro* and *in vivo* decarboxylation rates may be the result of an overestimation of the *in vitro* AAAD activity in striatal tissue from the release of AAAD from nondopaminergic neurons.[145,146] However, only 15% to 20% of AAAD in striatum has nondopaminergic origin.[147]
3. Can differences of $K_m$ and $V_{max}$ between L-DOPA (used *in vitro*) and FDOPA (used *in vivo*) as substrate for AAAD account for the differences? This is unlikely because $K_m$ and $V_{max}$ determined for FDOPA against AAAD (105 $\mu$M and 150 nmol/mm/g, respectively) are well within the range determined for L-DOPA (40–2000 $\mu$M and 33–150 nmol/mm/g, respectively). Equally important, *in vivo* PET determinations of $k'_3$ with L-[$\beta$-$^{11}$C]DOPA are also within the range of $k'_3$ values for FDOPA (Table 4-7[114,122–135]).
4. AAAD regulation *in vivo* may play a role because the enzyme needs a cofactor (pyridoxal phosphate) and its absence could be an inactivating mechanism for the enzyme.[148] Other biochemical and pharmacological modulating mechanisms have been identified in the

TABLE 4-8. Summary of Reported *In-Vitro* Aromatic-L-Aminoacid Decarboxylase (AAAD) Activity

| Species | Brain region | AAAD activity (ml/min/g) | Reference |
|---|---|---|---|
| Cat | Caudate | 0.215[a] | Kuntzman et al. (1961)[136] |
| Human (Postmortem) | Caudate | 0.057 | Mackay et al. (1978)[137] |
| Monkey (Green) | Putamen | — | Goldstein et al. (1969)[138] |
| Rat (Donryu) | Caudate | 0.107 | Rahman et al. (1981)[139] |
| Rat (Wistar) | Striatum | 0.447 | Broch and Fonnum (1972)[140] |
| Rat (Sprague–Dawley) | Striatum | 0.075 | Awapara and Saine (1975)[141] |
| Rat (Sprague–Dawley) | Striatum | 0.090 | Hefti et al. (1980)[142] |
| Rat (Hooded) | Striatum | 1.800 | Cumming et al. (1994)[135] |
| Rabbit | Caudate | 0.155 | McCaman et al. (1965)[143] |

*Source:* Reprinted with permission from Yee et al.[122]

[a]Unit conversion was carried out by dividing AAAD activity determined by the average $K_m$ for AAAD determined from pig kidney enzyme. The average $K_m$ used was 165 $\mu M$ as determined previously (Reprinted with permission from Reith et al.[133])

regulation of AAAD activity.[149] All these factors may be present *in vivo* and play a role in the down-regulation of AAAD.

5. Multiple compartmentalization of dopamine (and AAAD) within the neuron has been the subject of controversy.[150,151] Is it possible that because of this compartmentalization, the substrate (FDOPA) may have limited accessibility to AAAD *in vivo* and, therefore, the apparent $k_3$ determined with PET underestimates the true value? There is considerable evidence for and against these hypotheses in the literature.
6. Is there a limitation on FDOPA access to intraneuronal AAAD? This possibility has been initially suggested[117] and later demonstrated using synaptosomal preparations.[122] Transport restriction rationalizations are supported by the observations that L-DOPA (and FDOPA) are transported competitively across dopaminergic neurons (main competing amino acids are aromatic amino acids, such as phenylalanine, tyrosine, tryptophan) with KD = 2-5 $\mu M$, well below the Km of either L-DOPA or FDOPA for AAAD (about 100 $\mu M$, see above). Furthermore, to a lesser extent, L-DOPA (and FDOPA) transport across dopaminergic neurons is also subjected to competition by neutral aliphatic amino acids, like leucine, isoleucine and valine.

Thus, even though possibility (4) and (5) above cannot be entirely dismissed, the following conclusions can be established:

1. $k'_3$ (PET) AAAD decarboxylation determined with FDOPA-PET is limited by neuronal transport.
2. The specificity observed with FDOPA-PET for dopaminergic neurons in brain is determined in great measure by neuronal transport access to these terminals. Serotonin terminals also contain AAAD; however, the presence of the abundant aliphatic amino acids in plasma and brain tissue limits FDOPA access to these terminals.
3. These observations may explain results like the on-and-off phenomena in L-DOPA therapy in Parkinson's disease. This clinical effect relates to the apparent lack and resumption of response that Parkinson's patients may have to L-DOPA therapy, particularly af-

ter prolonged treatments. These phenomena may occur because delivery of L-DOPA to the remaining, active central dopaminergic terminals in these patients may be restricted by regulation of gene expression of neuronal aminoacid transporter proteins, coupled with severe competition with plasma amino acids, particularly at the level of the neuronal membrane.

## MOLECULAR IMAGING AND DRUG DEVELOPMENT

Many examples of molecular probes used with PET and discussed above have originated from drugs developed by the pharmaceutical industry. The marriage of molecular diagnostics with molecular therapeutics in the field was mainly nurtured by the existence of excellent drugs that target enzymes and receptors that were later adapted as molecular imaging probes. As a result of this interaction, many drug-mimicking imaging probes were developed and their utilization with PET provided insight into their site of action and their time-dependent interaction with these sites. In this regard, earlier advances focused on the design of procedures to define the relationship between plasma levels of drugs and receptor occupancy at the site of action in tissue.[152,153]

Receptor occupancy has been defined as the fraction (%) of the receptor population that is occupied by the unlabeled drug.[152] Because the binding of the imaging probe is stoichiometric and based on saturation kinetics, at high-specific activity the radiolabeled probe occupies only a minimum number of receptor sites. Therefore, when a drug binding to the same site is present, binding of the site by the molecular imaging probe will be reduced based on the amount of unlabeled drug present, its binding affinity for the target (KD), and the number of receptor sites (Bmax).

Receptor occupancy determinations have been made with a number of neuroreceptor probes which have provided an accurate view of the necessary dose of a drug for optimal clinical efficacy and reduced toxicity (Table 4-9).[153] The method has been most extensively applied to the determination of antipsychotic drugs binding.[152] For example, as a result of the utilization of this technique with PET, it was determined that neuroleptic action requires 70% to 80% dopamine-D2 receptor occupancy. Higher receptor occupancy, associated with overdosing, is also frequently associated with side effects involving disturbances of the motor system (extrapyramidal syndromes). Therefore PET is an important tool to optimize patient dose by measuring the target receptor occupancy. Figure 4-18[152] illustrates this principle.

With the advent of microPET cameras (Chapter 1), the use of PET has expanded to drug development,[42] initiated by combining the resources of the pharmaceutical industry with those of the radiopharmaceutical industry, universities, and government facilities. It is anticipated that this continued effort will

**TABLE 4-9. Neuroreceptor Quantitation and Occupancy Sites**

| *Drug/Imaging probe* | *Receptor site* |
|---|---|
| MDL-100, 907/N-[C-11]methylspiperone | 5-HT2A receptors |
| Clomipramine/F-18 setoperone | 5-HT2A receptors |
| Nalnefene/[C-11]carfentanil | Opiate receptors |
| SDZ MAR 327/[C-11] SCH 23390 | Dopamine $D_1$ receptors |

*Source:* Reprinted from Burns et al.,[153] with permission from Elsevier.

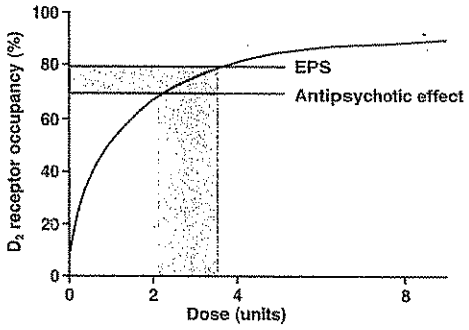


**FIGURE 4-18.** Suggested distinct thresholds for antipsychotic effects and extrapyramidal syndromes as induced by classical antipsychotic drugs, determined from PET measurement of receptor occupancy. Owing to the hyperbolic relationship between occupancy of the $D_2$ receptor and dose of antipsychotic drug (or plasma concentration), there is a rather narrow interval for optimal therapeutic treatment. Abbreviation: EPS, extrapyramidal syndromes. (Reprinted from Farde,[152] with permission from Elsevier.)

have a profound impact on the process of drug discovery and evaluation, reducing cost, and the time necessary to produce successful drugs for patient care. Such an approach is described in Figure 4-19.

Using the same technology as the one used to produce drugs (i.e., automated devices that perform combinatorial chemistry on solid support), combinatorial radiochemistry has proven effective in producing radiolabeled drugs. This technique, with a single radiolabeled reagent (i.e., C-11 methyl iodide), makes it possible to label large numbers of compounds identical to drug products or as analogs to be tested with microPET technology in mice and humans (Figure 4-20). These approaches will also be explored with other positron-emitting radioisotopes (e.g., F-18). Advantages of this approach include:

1. The solid-phase technology permits easy preparation of these radiolabeled drugs without purification because the only released product is the radiolabeled drug (i.e., Hoffman elimination).
2. MicroPET evaluation of drug candidates in mice (i.e., time-dependent organ distribution, plasma and cell membrane permeability, and mode of excretion) allows for the determination of structural predictors of *in-vivo* behavior based on specific physicochemical properties of these molecules (e.g., partition coeficient, a measure of the affinity of a compound for lipid environments).[154]

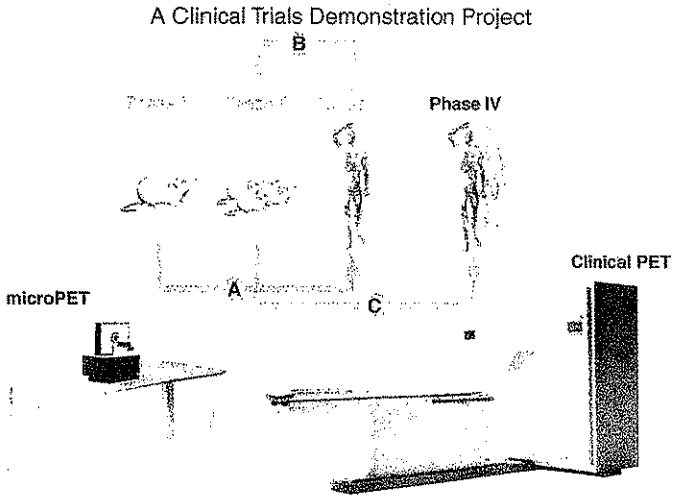


**FIGURE 4-19.** Model approach for discovery and evaluation of molecular imaging probes and drugs. A small number of animal models of disease are evaluated with microPET and molecular imaging probes and with direct biological assays and behavioral assessments. If results are positive, a small number of studies is performed in patients to assess the correlation between animal model and humans (A). In this case, a clinical PET scanner is used to perform the same assays in humans as were performed with microPET in animals. If the correlation is reasonable, larger numbers of animals are studied to better define the properties of the imaging probe or drug (B). A larger number of patient studies are then performed to evaluate an approach in humans with clinical PET (C), which could be used for evaluating drugs or molecular imaging probes.

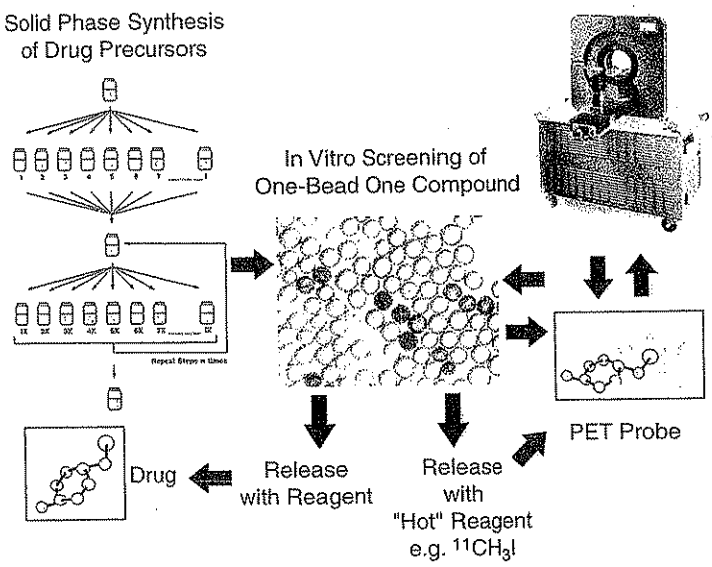


**FIGURE 4-20.** Schematic representation describing the marriage of combinatorial chemistry approaches in drug development and their use to produce radiolabeled versions of those drugs (PET probe) for *in vivo* evaluation with microPET in mice. This concept introduces PET in the early stages for *in vivo* evaluation of promising drug candidates.

It will also allow for the determination of the pharmacokinetic parameters associated with the mode of administration and the *in-vivo* affinity of drug candidates for tissue targets. By a commodity of methods used, microPET study paradigms are then translated to human patients with clinical PET scanners.

3. The data base on the *in-vivo* distribution of drug candidates will facilitate the computational design of new combinatorial libraries using, for example,

**EXAMPLE 4-11**

In addition to the examples given above, describe *specifically* how PET can be used in the process of drug discovery.

**ANSWER**

The genome and protein sequencing is increasing the number of targets (i.e., receptors, enzymes, messenger RNA, and genes) for pharmaceutical intervention. The pharmaceutical industry has addressed this challenge by developing combinatorial chemical technology that now permits the synthesis of millions of molecules for specific targets in short periods of time. Microarray and cell culture testing technology has been developed for *in vitro* assay of the biological properties of these compounds for these targets. What is limiting the drug discovery process is high throughput *in vivo* biological screening and *in vivo* testing, a process complicated by the large number of compounds to be tested and the lack of technologies to perform biological screening in living mammals, from mice to humans. The use of labeled drugs and other molecular imaging probes to assess alterations in the biological process targeted by the drug provides the means through microPET and PET to evaluate pharmacokinetics, pharmacodynamics, transport from plasma to tissue, and tissue target occupancy.

pharmacophore fingerprinting[155] based on specific chemical features of the molecules. The application of computational tools to identify structural correlates of *in-vivo* data using various algorithms (i.e., computational informatics) will then: 1) enable the development of predictors of *in-vivo* behavior, 2) increase the likelihood of success when drug candidates are used in humans (clinical trials), and 3) accelerate the drug discovery process.

The combination of all these features, including rapid radiolabeling of thousands of molecules and their *in-vivo* evaluation in rodents, has the power to alter the dynamics of combinatorial chemistry design. It will also allow the rapid introduction of selective, promising drug candidates into rodents, nonhuman primates, and humans using the same radiolabeling concept. Therefore, the energy barrier for introduction of these drugs into clinical trials (Figure 4-19) will be reduced and, most importantly, a much more accurate and scientifically based selection and evaluation of candidate drugs will be achieved.

## MAKING MOLECULAR IMAGING PROBES AVAILABLE VIA DISTRIBUTION CENTERS

In the late 1970s and early 1980s, enormous progress was made in the development of PET technology as a result of generous government support in the United States (i.e., Department of Energy and the National Institutes of Health) and abroad. This support resulted in: 1) the development of new cyclotron technology for biomedical use (Chapter 3); 2) synthesis of a wide array of biological imaging probes; 3) design and engineering of new automated synthesis integrated with the new cyclotron technology to yield a new concept of electronic generators (Chapter 3); and 4) new technological developments in instrumentation, leading to high-resolution tomographs (Chapter 1). Research in humans intensified and new observations on the biochemistry of disease, coupled with the technological innovations previously mentioned, paved the way for the clinical utilization of PET. The Food and Drug Administration Modernization Act of 1997[156] also provided the legal basis for a new regulatory paradigm for clinical PET and reimbursement for clinical applications of PET in cancer, as well as neurological and cardiovascular diseases.

Making PET available to patients would not have been possible without radiopharmacy distribution centers, a service that emerged in the mid 1990s and has grown very rapidly since then. Today, FDG, the main radiopharmaceutical used in clinical PET, is available throughout the United States and many parts of Canada, Europe, Japan, Asia, South America, and Australia because of the expansion of these radiopharmaceutical services. However, a new phenomenon is occurring as a result of progress in two major areas: 1) the development of microPET technology (Chapter 1), which has made PET accessible to biological scientists and physicians working on the molecular basis of disease; and 2) the aggressive introduction of the pharmaceutical industry in the field, alerted to the value of PET in the process of drug discovery. The relationship between PET and the pharmaceutical industry provides great value to each. To PET, the pharmaceutical industry provides access to their molecular syntheses, screening technologies, and molecular libraries. To the pharmaceutical industry, PET provides a means to biological screen and evaluate drugs in living mammals, from genetically engineered and human cell transplant models of disease to the ultimate laboratory setting of the patient.

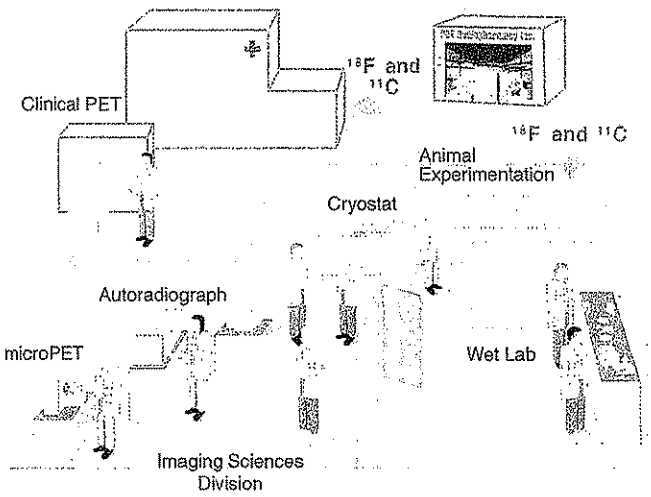


**FIGURE 4-21.** Relationship between clinical PET services and research and development of PET radiopharmaceuticals. In this model, PET radiopharmacy delivers Food and Drug Administration-approved PET radiopharmaceuticals to clinics. PET radiopharmaceuticals and radioisotopes are also delivered to imaging research laboratories with small-animal imaging modalities such as PET, MRI, single photon emission computed tomography (SPECT), CT, autoradiography, optical imaging systems, and wet laboratories for tissue, cell, and chemical analysis. These laboratories are in universities, radiopharmaceutical companies, or pharmaceutical companies and can focus on discovery of molecular imaging probes or pharmaceuticals or both together. Outcomes are translated into clinical research and, then, clinical practice.

Thus, the concept of integrated PET centers is evolving. The clinician operating a clinical PET service is no longer the only customer of the PET radiopharmacy. The need to make molecular imaging probes (i.e., for transgene expression determinations in animals or drug-mimicking probes) available through distribution centers has become indispensable for rapid growth of PET through biological and pharmacologic research in the new areas of molecular medicine. The delivery of positron-emitting radioisotopes and labeled compounds is indeed similar to the commercial delivery of C-14, H-3, P-32, and I-125 radioisotopes and labeled compounds to research laboratories.

In this new model, several alternatives are evolving, including availability and delivery of: 1) PET radiopharmaceuticals for diagnostic use; 2) imaging probes to research laboratories in hospitals, universities, and the pharmaceutical industry with microPET and PET tomographs for human use; and 3) chemistry precursors to these laboratories. The latter is a convenient avenue for sites that, having access to nearby PET radiopharmacies, may obtain the necessary radiolabeled precursor (i.e., fluoride ion) to prepare PET imaging probes or to labeled experimental probes. This process facilitates new investigations and opens novel pathways from probe discovery to clinical use (Figure 4-21).

## REFERENCES

1. Webster's Encyclopedic Unabridged Dictionary of the English Language. New York: Gramercy Books; 1996;564.
2. Mazziotta JC, Phelps ME. In: Phelps ME, Mazziotta JC, Schelbert HR, eds. *Positron Emission Tomography Studies of the Brain in Positron Emission Tomography and Autography.* New York: Raven Press; 1986.
3. Small GW, Ercoli LM, Silverman DHS, et al. Cerebral metabolic and cognitive decline in persons at genetic risk for Alzheimer's disease. *Proc Natl Acad Sci USA.* 2000;97:6037–6042.
4. Huang S-C, Phelps ME. In: Phelps ME, Mazziotta JC, Schelbert HR, eds. *Positron Emission Tomography and Autoradiography: Principles and Applications.* New York: Raven Press; 1986;287–346.

4A. Huang S-C, Barrio JR, Phelps ME. Neuroreceptor assay with positron emission tomography: equilibrium versus dynamic approaches. *J Cereb Blood Flow Metab.* 1986;6:515–521.

5. Welch R, ed. *The Fluctuating Enzyme.* New York: John Wiley and Sons; 1986.

6. Sokoloff L, Reivich M, Kennedy C, et al. The [14C]deoxyglucose method for the measurement of local cerebral glucose utilization: theory, procedure, and normal values in the conscious and anesthetized albino rat. *J Neurochem.* 1977;28:897–916.
7. Sokoloff L. In: Phelps ME, Mazziotta JC, Schelbert HR, eds. *Positron Emission Tomography and Autoradiography.* New York: Raven Press; 1986;1–72.
8. Huang S-C, Phelps ME, Hoffman EJ, et al. Noninvasive determination of local cerebral metabolic rate of glucose in man. *Am J Physiol.* 1980;238:E69–E82.
9. Reivich M, Alavi A, Wolf A, et al. Glucose metabolic rate kinetic model parameter determination in humans: the lumped constants and rate constants for [$^{18}$F]fluorodeoxyglucose and [11C]deoxyglucose. *J Cereb Blood Flow Metab.* 1985;5:179–192.
10. Hasselbalch SG, Knudsen GM, Madsen PL, et al. Calculation of the FDG lumped constants by extraction fractions of FDG and glucose. *J Cereb Blood Flow Metab.* 1997;17:S440.
11. Hasselbalch SG, Madsen PL, Knudsen GM, et al. Calculation of the FDG lumped constant by simultaneous measurements of global glucose and FDG metabolism in humans. *J Cereb Blood Flow Metab.* 1998;18:154–160.
12. Spence AM, Muzi M, Graham MM, et al. Glucose metabolism in human malignant gliomas measured quantitatively with PET, 1-[C-11]glucose and FDG: analysis of the FDG lumped constant. *J Nucl Med.* 1998;39:440–448.
13. Wu HM, Bergsneider M, Yeh E, et al. XXth International Symposium on Cerebral Blood Flow and Metabolism, Taipei, Taiwan, 2001.
14. Suda S, Shinohara M, Miyaoka M, et al. Local cerebral glucose utilization in hypoglycemia. *J Cereb Blood Flow Metab.* 1981;1:S62.
15. Siesjo BK. *Brain Energy Metabolism.* New York: John Wiley & Sons; 1978.
16. Bessell EM, Thomas P. The effect of substitution at C-2 of D-glucose 6-phosphate on the rate of dehydrogenation by glucose 6-phosphate dehydrogenase (from yeast and from rat liver). *Biochem J.* 1973;13:83–89.
17. Phelps ME, Huang SC, Hoffman EJ, et al. Tomographic measurement of local cerebral glucose metabolic rate in humans with (F-18)2-fluoro-2-deoxy-D-glucose: validation of method. *Ann Neurol.* 1979;6:371–388.
18. Bessell EM, Foster AB, Westwood JH. The use of deoxyfluoro-D-glucopyranoses and related compounds in a study of yeast hexokinase specificity. *Biochem J.* 1972;128:199–204.
19. Walsh C. In: Meister A, ed. *Advances in Enzymology.* New York: John Wiley & Sons; 1983;55:197–289.
20. Sols A, Crane RK. Substrate specificity of brain hexokinase. *J Biol Chem.* 1954;210:581–595.
21. Langen P, Etzold G, Hintsche R, et al. 3′-deoxy-3′-fluorothymidine, a new selective inhibitor of DNA-synthesis. *Acta Biol Med Ger.* 1969;23:759–766.
22. Kong X-B, Zhu Q-Y, Vidal PM, et al. Comparisons of anti-human immunodeficiency virus activities, cellular transport, and plasma and intracellular pharmacokinetics of 3′-fluoro-3′-deoxythymidine and 3′-azido-3′-deoxythymidine. *Antimicrob Agents Chemother.* 1992;36:808–818.
23. Matthes E, Lehmann CH, Scholz D, et al. Inhibition of HIV-associated reverse transcriptase by sugar-modified derivatives of thymidine 5′-triphosphate in comparison to cellular DNA polymerases alpha and beta. *Biochem Biophys Res Commun.* 1987;148:78–85.
24. Sundseth R, Joyner SS, Moore JT, et al. The anti-human immunodeficiency virus agent 3′-fluorothymidine induces DNA damage and apoptosis in human lymphoblastoid cells. *Antimicrob Agents Chemother.* 1996;40:331–335.
25. Grierson JR, Shields AF. Radiosynthesis of 3′-deoxy-3′-[(18)F]fluorothymidine: [(18)F] FLT for imaging of cellular proliferation in vivo. *Nucl Med Biol.* 2000;27:143–156.
26. Shields AF, Grierson JR, Muzik O, et al. Kinetics of 3′-deoxy-3′-[F-18]flurorthymidine uptake and retention in dogs. *Mol Imag Biol.* 2002;4:83–90.
27. Shields AF, Grierson JR, Dohmen BM, et al. Imaging proliferation in vivo with [F-18]FLT and positron emission tomography. *Natl Med.* 1998;4:1334–1336.
28. DeGrado TR, Coleman RE, Baldwin SW, et al. [$^{18}$F ]flurocholine (FCH) as an oncologic PET tracer: evaluation in murine prostate cancer xenograft model. *J Nucl Med.* 2000;41:231P.
29. Friedland RP, Mathis CA, Budinger TF, et al. Labeled choline and phosphorylcholine: body distribution and brain autoradiography: concise communication. *J Nucl Med.* 1983;24:812–815.
30. Hara T, Kosaka N, Shinoura N, et al. PET imaging of brain tumor with [methyl-11C]choline. *J Nucl Med.* 1997;38:842–847.
31. Shinoura N, Nishijima M, Hara T, et al. Brain tumors: detection with C-11 choline PET. *Radiology.* 1997;202:497–503.

32. Hara T, Kosaka N, Kishi H. PET imaging of prostate cancer using carbon-11-choline. *J Nucl Med.* 1998;39:990–995.
33. Kobori O, Kirihara Y, Kosaka N, et al. Positron emission tomography of esophageal carcinoma using (11)C-choline and (18)F-fluorodeoxyglucose: a novel method of preoperative lymph node staging. *Cancer.* 1999;86:1638–1648.
34. Clary GL, Tsai C-F, Guynn RW. Substrate specificity of choline kinase. *Arch Biochem Biophys.* 1987;254:214–221.
35. Alcoceba HR, Saniger L, Campos J, et al. Choline kinase inhibitors as a novel approach for antiproliferative drug design. *Oncogene.* 1997;15:2289–2301.
36. Gambhir SS, Barrio JR, Herschman HR, et al. Assays for noninvasive imaging of reporter gene expression. *Nucl Med Biol.* 1999;26:481–490.
37. Gambhir SS, Barrio JR, Herschman HR, et al. Imaging gene expression: principles and assays. *J Nucl Cardiol.* 1999;6:219–233.
38. Gambhir SS, Bauer E, Black ME, et al. A mutant herpes simplex virus type 1 thymidine kinase reporter gene shows improved sensitivity for imaging reporter gene expression with positron emission tomography. *Proc Natl Acad Sci USA.* 2000;97:2785–2790.
39. Yu Y, Annala AJ, Barrio JR, et al. Quantification of target gene expression by imaging reporter gene expression in living animals. *Natl Med.* 2000;6:933–937.
40. MacLaren DC, Toyokuni T, Cherry SR, et al. PET imaging of transgene expression. *Biol Psychiatry.* 2000;48:337–348.
41. Crooke ST, Lebleu B. *Antisense and Application.* Ann Arbor: CRC Press; 1993;579.
42. Phelps ME. PET: the merging of biology and imaging into molecular imaging. *J Nucl Med.* 2000;41:661–681.
43. Shi N, Boado RJ, Pardridge WM. Antisense imaging of gene expression in the brain in vivo. *Proc Natl Acad Sci USA.* 2000;97:14709–14714.
44. Fowler JS, MacGregor RR, Wolf AP, et al. Mapping human brain monoamine oxidase A and B with $^{11}$C-labeled suicide inactivators and PET. *Science.* 1987;235:481–485.
45. Abeles RH, Maycock AL. Suicide enzyme inactivators. *Acc Chem Res.* 1976;9:313.
46. Trojanowski JQ, Shin R-W, Schmidt ML. Relationship between plaques, tangles, and dystrophic processes in Alzheimer's disease. *Neurobiol Aging.* 1995;16:335–340.
47. Barrio JR, Huang S-C, Cole G, et al. PET imaging of tangles and plaques in Alzheimer's Disease with a highly hydrophobic probe. *J Label Compds Radiopharm.* 1997;42:S194–S195.
48. Shoghi-Jadid K, Small G, Agdeppa ED. Localization of neurofibrillary tangles and beta-amyloid plaques in the brains of living patients with Alzheimer disease. *Am J Geriatr Psychiatry.* 2002;10:24–35.
49. Agdeppa ED, Kepe V, Shoghi-Jadid K, et al. In vivo and in vitro labeling of plaques and tangles in the brain of an Alzheimer's Disease patient: a case study. *J Nucl Med.* 2001;42:65P.
50. Agdeppa ED, Kepe V, Petric A, et al. In vitro detection of (S)—naproxen and ibuprofen binding to plaques in the Alzheimer's brain using the PET molecular imaging probe [18F] FDDNP. *Neuroscience.* 2003;117:723–730.
51. Ray P, Bauer E, Iyer M, et al. Monitoring gene therapy with reporter gene imaging. *Semin Nucl Med.* 2001;31:312–320.
52. Haberkorn U, Oberdorfer F, Gebert J, et al. Monitoring gene therapy with cytosine deaminase: in vitro studies using tritiated-5-fluorocytosine. *J Nucl Med.* 1996;37:87–94.
53. Stegman LD, Rehemtulla A, Beattie B, et al. Noninvasive quantitation of cytosine deaminase transgene expression in human tumor xenografts with in vivo magnetic resonance spectroscopy. *Proc Natl Acad Sci USA.* 1999;96:9821–9826.
54. Tjuvajev JG, Finn R, Watanabe K, et al. Noninvasive imaging of herpes virus thymidine kinase gene transfer and expression: a potential method for monitoring clinical gene therapy. *Cancer Res.* 1996;56:4087–4095.
55. Tjuvajev JG, Chen SH, Joshi A, et al. Imaging adenoviral-mediated herpes virus thymidine kinase gene transfer and expression in vivo. *Cancer Res.* 1999;59:5186–5193.
56. Tjuvajev JG, Joshi A, Callegari J, et al. A general approach to the non-invasive imaging of transgenes using cis-linked herpes simplex virus thymidine kinase. *Neoplasia.* 1999;1:315–320.
57. Haubner R, Avril N, Hantzopoulos PA, et al. In vivo imaging of herpes simplex virus type 1 thymidine kinase gene expression: early kinetics of radiolabelled FIAU. *Eur J Nucl Med.* 2000;27:283–291.
58. Morin KW, Atrazheva ED, Knaus EE, et al. Synthesis and cellular uptake of 2′-substituted analogues of (E)-5-(2-[125I]iodovinyl)-2′-deoxyuridine in tumor cells trans-

duced with the herpes simplex type-1 thymidine kinase gene. Evaluation as probes for monitoring gene therapy. *J Med Chem.* 1997;40:2184–2190.
59. Wiebe LI, Knaus EE, Morin KW. Radiolabelled pyrimidine nucleosides to monitor the expression of HSV-1 thymidine kinase in gene therapy. *Nucleosides Nucleotides.* 1999; 18:1065–1066.
60. Germann C, Shields AF, Grierson JR, et al. 5-Fluoro-1-(2′-deoxy-2′-fluoro-beta-D-ribofuranosyl) uracil trapping in Morris hepatoma cells expressing the herpes simplex virus thymidine kinase gene. *J Nucl Med.* 1998;39:1418–1423.
61. Gambhir SS, Barrio JR, Wu L, et al. Imaging of adenoviral-directed herpes simplex virus type 1 thymidine kinase reporter gene expression in mice with radiolabeled ganciclovir. *J Nucl Med.* 1998;39:2003–2011.
62. Haberkorn U, Altmann A, Morr I, et al. Monitoring gene therapy with herpes simplex virus thymidine kinase in hepatoma cells: uptake of specific substrates. *J Nucl Med.* 1997;38:287–294.
63. Haberkorn U, Khazaie K, Morr I, et al. Ganciclovir uptake in human mammary carcinoma cells expressing herpes simplex virus thymidine kinase. *Nucl Med Biol.* 1998;25:367–373.
64. Iyer M, Barrio JR, Namavari M, et al. 8-[$^{18}$F]Fluoropenciclovir: an improved reporter probe for imaging HSV1-tk reporter gene expression in vivo using PET. *J Nucl Med.* 2001;42:96–105.
65. Alauddin MM, Conti PS, Mazza SM, et al. 9-[(3-[$^{18}$F]-fluoro-1-hydroxy-2-propoxy)-methyl] guanine ([$^{18}$F]-FHPG): a potential imaging agent of viral infection and gene therapy using PET. *Nucl Med Biol.* 1996;23:787–792.
66. Alauddin MM, Shahinian A, Kundu RK, et al. Evaluation of 9-[(3-$^{18}$F -fluoro-1-hydroxy-2-propoxy)methyl]guanine ([$^{18}$F]-FHPG) in vitro and in vivo as a probe for PET imaging of gene incorporation and expression in tumors. *Nucl Med Biol.* 1999;26:371–376.
67. de Vries EFJ, van Waarde A, Harmsen MC, et al. [(11)C]FMAU and [(18)F]FHPG as PET tracers for herpes simplex virus thymidine kinase enzyme activity and human cytomegalovirus infections. *Nucl Med Biol.* 2000;27:113–119.
68. Hospers GAP, Calogero A, van Waarde A, et al. Monitoring of herpes simplex virus thymidine kinase enzyme activity using positron emission tomography. *Cancer Res.* 2000;60:1488–1491.
69. Hustinx R, Shiue CY, Alavi A, et al. Imaging in vivo herpes simplex virus thymidine kinase gene transfer to tumour-bearing rodents using positron emission tomography *Eur J Nucl Med.* 2001;28:5–12.
70. Alauddin MM, Conti PS. Synthesis and preliminary evaluation of 9-(4-[$^{18}$F]-fluoro-3-hydroxymethylbutyl)guanine ([$^{18}$F ]FHBG): a new potential imaging agent for viral infection and gene therapy using PET. *Nucl Med Biol.* 1998;25:175–180.
71. Yaghoubi S, Barrio JR, Dahlbom M, et al. Human pharmacokinetic and dosimetry studies of [(18)F]FHBG: a reporter probe for imaging herpes simplex virus type-1 thymidine kinase reporter gene expression. *J Nucl Med.* 2001;42:1225–1234.
72. Sun X, Annala A, Yaghoubi S, et al. Quantitative imaging of gene induction in living animals. *Gene Ther.* 2001;8:1572–1579.
73. MacLaren DC, Gambhir SS, Satyamurthy N, et al. Repetitive, non-invasive imaging of the dopamine D2 receptor as a reporter gene in living animals. *Gene Ther.* 1999;6:785–791.
74. Yaghoubi SS, Wu L, Liang Q, et al. Direct correlation between positron emission tomographic images of two reporter genes delivered by two distinct adenoviral vectors. *Gene Ther.* 2001;8:1072–1080.
75. Liang Q, Satyamurthy N, Barrio JR, et al. Noninvasive, quantitative imaging in living animals of a mutant dopamine D2 receptor reporter gene in which ligand binding is uncoupled from signal transduction. *Gene Ther.* 2001;8:1490–1498.
76. Rogers BE, McLean SF, Kirkman RL, et al. In vivo localization of [(111)In]-DTPA-D-Phe1-octreotide to human ovarian tumor xenografts induced to express the somatostatin receptor subtype 2 using an adenoviral vector. *Clin Cancer Res.* 1999;5:383–393.
77. Buchsbaum DJ, Rogers BE, Khazaeli MB, et al. Targeting strategies for cancer radiotherapy. *Clin Cancer Res.* 1999;5:3048s–3055s.
78. Rogers BE, Zinn KR, Buchsbaum DJ. Noninvasive monitoring of gene transfer using a reporter receptor imaged with a high-affinity peptide radiolabeled with 99mTc or 188Re. *J Nucl Med.* 2000;41:887–895.
79. Zinn KR, Buchsbaum DJ, Chaudhuri TR, et al. Noninvasive monitoring of gene transfer using a reporter receptor imaged with a high-affinity peptide radiolabeled with 99mTc or 188Re. *J Nucl Med.* 2000;41:887–895.

80. Bogdanov A Jr., Petherick P, Marecos E, et al. In vivo localization of diglycylcysteine-bearing synthetic peptides by nuclear imaging of oxotechnetate transchelation. *Nucl Med Biol.* 1997;24:739–742.
81. Bogdanov A Jr., Simonova M, Weissleder R. Design of metal-binding green fluorescent protein variants. *Biochim Biophys Acta.* 1998;1397:56–64.
82. Baidoo KE, Scheffel U, Stathis M, et al. High-affinity no-carrier-added 99mTc-labeled chemotactic peptides for studies of inflammation in vivo. *Bioconjug Chem.* 1998;9:208–217.
83. Rogers BE, Curiel DT, Mayo MS, et al. Tumor localization of a radiolabeled bombesin analogue in mice bearing human ovarian tumors induced to express the gastrin-releasing peptide receptor by an adenoviral vector. *Cancer.* 1997;80:2419–2424.
84. Rogers BE, Rosenfeld ME, Khazaeli MB, et al. Localization of iodine-125-mIP-Des-Met14-bombesin (7-13)NH2 in ovarian carcinoma induced to express the gastrin releasing peptide receptor by adenoviral vector-mediated gene transfer. *J Nucl Med.* 1997;38:1221–1229.
85. Rosenfeld ME, Rogers BE, Khazaeli MB, et al. Adenoviral-mediated delivery of gastrin-releasing peptide receptor results in specific tumor localization of a bombesin analogue in vivo. *Clin Cancer Res.* 1997;3:1187–1194.
86. Boland A, Ricard M, Opolon, P, et al. Adenovirus-mediated transfer of the thyroid sodium/iodide symporter gene into tumors for a targeted radiotherapy. *Cancer Res.* 2000;60:3484–3492.
87. Haberkorn U, Henze M, Altmann A, et al. Transfer of the human NaI symporter gene enhances iodide uptake in hepatoma cells. *J Nucl Med.* 2001;42:317–325.
88. Enochs WS, Petherick P, Bogdanova A, et al. Paramagnetic metal scavenging by melanin: MR imaging. *Radiology.* 1997;204:417–423.
89. Weissleder R, Simonova M, Bogdanova A, et al. MR imaging and scintigraphy of gene expression through melanin induction. *Radiology.* 1997;204:425–429.
90. Hasgawa S, Yang M, Chishima T, et al. In vivo tumor delivery of the green fluorescent protein gene to report future occurrence of metastasis. *Cancer Gene Ther.* 2000;7:1336–1340.
91. Pfeifer A, Kessler T, Yang M, et al. Transduction of liver cells by lentiviral vectors: analysis in living animals by fluorescence imaging. *Mol Ther.* 2001;3:319–322.
92. Yang M, Baranov E, Jiang P, et al. Whole-body optical imaging of green fluorescent protein-expressing tumors and metastases. *Proc Natl Acad Sci USA.* 2000;97:1206–1211.
93. Yang M, Baranov E, Li XM, et al. Whole-body and intravital optical imaging of angiogenesis in orthotopically implanted tumors. *Proc Natl Acad Sci USA.* 2001;98:2616–2621.
94. Yang M, Hasegawa S, Jiang P, et al. Visualizing gene expression by whole-body fluorescence imaging. *Proc Natl Acad Sci USA.* 2000;97:12278–12282.
95. Yang M, Hasegawa S, Jiang P, et al. Widespread skeletal metastatic potential of human lung cancer revealed by green fluorescent protein expression. *Cancer Res.* 1998;58:4217–4221.
96. Yang M, Jiang P, Sun FX, et al. A fluorescent orthotopic bone metastasis model of human prostate cancer. *Cancer Res.* 1999;59:781–786.
97. Contag CH, Spilman SD, Contag PR, et al. Visualizing gene expression in living mammals using a bioluminescent reporter. *Photochem Photobiol.* 1997;66:523–531.
98. Contag PR, Olomu IN, Stevenson DK, et al. Bioluminescent indicators in living mammals. *Natl Med.* 1998;4:245–247.
99. Bhaumik S, Gambhir SS. Optical imaging of Renilla luciferase reporter gene expression in living mice. *Proc Natl Acad Sci USA.* 2002;99:377–382.
100. Tung CH, Bredow S, Mahmood U, et al. Preparation of a cathepsin D sensitive near-infrared fluorescence probe for imaging. *Bioconjug Chem.* 1999;10:892–896.
101. Tung CH, Mahmood U, Bredow S, et al. In vivo imaging of proteolytic enzyme activity using a novel molecular reporter. *Cancer Res.* 2000;60:4953–4958.
102. Weissleder R, Tung CH, Mahmood U, et al. In vivo imaging of tumors with protease-activated near-infrared fluorescent probes. *Nat Biotechnol.* 1999;17:375–378.
103. Louie AY, Huber MM, Ahrens ET, et al. In vivo visualization of gene expression using magnetic resonance imaging. *Nat Biotechnol.* 2000;18:321–325.
104. Weissleder R, Moore A, Mahmood U, et al. In vivo magnetic resonance imaging of transgene expression. *Natl Med.* 2000;6:351–355.
105. Shand M, Weber F, Mariani L, et al. A phase 1-2 clinical trial of gene therapy for recurrent glioblastoma multiforme by tumor transduction with the herpes simplex thymidine kinase gene followed by ganciclovir. GLI328 European-Canadian Study Group. *Human Gene Ther.* 1999;10:2325–2335.
106. Aghi M, Ting CC, Suling K, et al. Multimodal cancer treatment mediated by a replicating oncolytic virus that delivers the oxazaphosphorine/rat cytochrome P450 2B1 and ganciclovir/herpes simplex virus thymidine kinase gene therapies. *Cancer Res.* 1999;59:3861–3865.

107. Engelmann C, Panis Y, Bolard J, et al. Liposomal encapsulation of ganciclovir enhances the efficacy of herpes simplex virus type 1 thymidine kinase suicide gene therapy against hepatic tumors in rats. *Human Gene Ther.* 1999;10:1545–1551.
108. Kim B, Loeb LA. A screen in Escherichia coli for nucleoside analogs that target human immunodeficiency virus (HIV) reverse transcriptase: coexpression of HIV reverse transcriptase and herpes simplex virus thymidine kinase. *J Virol.* 1995;69:6563–6566.
109. Caruso M, Salomon B, Zhang S, et al. Expression of a Tat-inducible herpes simplex virus-thymidine kinase gene protects acyclovir-treated CD4 cells from HIV-1 spread by conditional suicide and inhibition of reverse transcription. *Virology.* 1995;206:495–503.
110. Bradshaw HD Jr., Deininger PL. Human thymidine kinase gene: molecular cloning and nucleotide sequence of a cDNA expressible in mammalian cells. *Mol Cell Biol.* 1984;4:2316–2320.
111. Pilger BD, Perozzo R, Albers F, et al. Substrate diversity of herpes simplex virus thymidine kinase. Impact of the kinematics of the enzyme. *J Biol Chem.* 1999;274:31967–31973.
112. Champness JN, Bennett MS, Wien F, et al. Exploring the active site of herpes simplex virus type-1 thymidine kinase by X-ray crystallography of complexes with aciclovir and other ligands. *Proteins.* 1998;32:350–361.
113. Alauddin MM, Conti PS, Mazza SM, et al. Synthesis of F-18 9-[(3-fluoro-1-hydroxy-2-propoxy)-methyl]-guanine (FHPG) for in vivo imaging of viral infection and gene therapy with PET. *J Nucl Med.* 1996;37:193P.
114. Barrio JR, Huang S-C, Yu D-C, et al. Radiofluorinated L-m-tyrosines: new in-vivo probes for central dopamine biochemistry. *J Cereb Blood Flow Metab.* 1996;16:667–678.
115. Herschman HR, Barrio JR, Satyamurthy N, et al. In: Curiel DR, Douglas JT, eds. *Monitoring Gene Therapy by Positron Emission Tomography.* New York: Wiley-Liss, Inc. 2002;661–689.
116. Pike VW, Halldin C, Wikstrom H, et al. Radioligands for the study of brain 5-HT(1A) receptors in vivo-development of some new analogues of way. *Nucl Med Biol.* 2000;27:449–455.
117. Barrio JR, Huang S-C, Phelps ME. Biological imaging and the molecular basis of dopaminergic diseases. *Biochem Pharmacol.* 1997;54:341–348.
118. Michael AC, Justice JB Jr., Neill DB. In vivo voltammetric determination of the kinetics of dopamine metabolism in the rat. *Neurosci Lett.* 1985;56:365–369.
119. Wood PL, Kim HS, Stocklin K, et al. Dynamics of the striatal 3-MT pool in rat and mouse: species differences as assessed by steady-state measurements and intracerebral dialysis. *Life Sci.* 1988;42:2275–2281.
120. Shoghi-Jadid K, Huang S-C, Stout DB, et al. Striatal kinetic modeling of FDOPA with a cerebellar-derived constraint on the distribution of volume of 30MFD: a PET investigation using non-human primates. *J Cereb Blood Flow Metab.* 2000;20:1134–1148.
121. Nissbrandt H, Carlsson A. Turnover of dopamine and dopamine metabolites in rat brain: comparison between striatum and substantia nigra. *J Neurochem.* 1987;49:959–967.
122. Yee RE, Huang S-C, Stout DB, et al. Nigrostriatal reduction of aromatic L-amino acid decarboxylase activity in MPTP-treated squirrel monkeys: in vivo and in vitro investigations. *J Neurochem.* 2000;74:1147–1157.
123. Gjedde A, Reith J, Dyne S, et al. Dopa decarboxylase activity of the living human brain. *Proc Natl Acad Sci USA.* 1991;88:2721–2725.
124. Huang S-C, Yu D-C, Barrio JR, et al. Kinetics and modeling of L-6-[$^{18}$F]fluoro-dopa in human positron emission tomographic studies. *J Cereb Blood Flow Metab.* 1991;11:898–913.
125. Hoshi H, Kuwabara H, Leger G, et al. 6-[$^{18}$F]fluoro-L-dopa metabolism in living human brain: a comparison of six analytical methods. *J Cereb Blood Flow Metab.* 1993;13:57–69.
126. Ishikawa T, Dhawan V, Chaly T, et al. Clinical significance of striatal DOPA decarboxylase activity in Parkinson's disease. *J Nucl Med.* 1996;37:216–222.
127. Kuwabara H, Cumming P, Yasuhara Y, et al. Regional striatal DOPA transport and decarboxylase activity in Parkinson's disease. *J Nucl Med.* 1995;36:1226–1231.
128. Wahl L, Nahmias C. Modeling of fluorine-18-6-fluoro-L-dopa in humans. *J Nucl Med.* 1996;37:432–437.
129. Nahmias C, Wahl L, Chirakal R, et al. A probe for intracerebral aromatic amino-acid decarboxylase activity: distribution and kinetics of [$^{18}$F]6-fluoro-L-m-tyrosine in the human brain. *Mov Disord.* 1995;10:298–304.
130. Barrio JR, Huang S-C, Melega WP, et al. 6-[$^{18}$F]fluoro-L-dopa probes dopamine turnover rates in central dopaminergic structures. *J Neurosci Res.* 1990;27:487–93.
131. Hartvig P, Tedroff J, Lindner KJ, et al. Positron emission tomographic studies on aromatic L-amino acid decarboxylase activity in vivo for L-dopa and 5-hydroxy-L-tryptophan in the monkey brain. *J Neural Transm Gen Sect.* 1993;94:127–135.

132. Tsukada H, Lindner KJ, Hartvig P, et al. Effect of 6R-L-erythro-5,6,7,8-tetrahydrobiopterin and infusion of L-tyrosine on the in vivo L-[beta-11C] DOPA disposition in the monkey brain. *Brain Res.* 1996;713:92–98.
133. Reith J, Dvye S, Kuwabara H, et al. Blood-brain transfer and metabolism of 6-[$^{18}$F]fluoro-L-dopa in rat. *J Cereb Blood Flow Metab.* 1990;10:707–719.
134. Cumming P, Kuwabara H, Ase A, et al. Regulation of DOPA decarboxylase activity in brain of living rat. *J Neurochem.* 1995;65:1381–1390.
135. Cumming P, Kuwabara H, Gjedde A. A kinetic analysis of 6-[$^{18}$F]fluoro-L-dihydroxyphenylalanine metabolism in the rat. *J Neurochem.* 1994;63:1675–1682.
136. Kuntzman R, Shore PA, Bogdanshi D, et al. Microanalytical procedures for fluorometric assay if brain dopa-5HTP decarboxylase, norepinephrine, and seratonin, and a detailed mapping of decarboxylase activity in brain. *J Neurochem.* 1961;6:226–232.
137. Mackay AVP, Davis P, Dewar AJ, et al. Regional distribution of enzymes associated with neurotransmission by monoamines, acetylcholine and GABA in the human brain. *J Neurochem.* 1978;30:827–839.
138. Goldstein M, Anagnoste B, Battista AF, et al. Studies of amines in the striatum in monkeys with nigral lesions. The disposition, biosynthesis and metabolites of [3H]dopamine and [14C]serotonin in the striatum. *J Neurochem.* 1969;16:645–653.
139. Rahman MK, Nagatsu T, Kato T. Aromatic L-amino acid decarboxylase activity in central and peripheral tissues and serum of rats with L-DOPA and L-5-hydroxytryptophan as substrates. *Biochem Pharmacol.* 1981;30:645–649.
140. Broch OJ Jr., Fonnum F. The regional and subcellular distribution of catechol-O-methyl transferase in the rat brain. *J Neurochem.* 1972;19:2049–2055.
141. Awapara J, Saine S. Fluctuations in DOPA decarboxylase activity with age. *J Neurochem.* 1975;24:817–818.
142. Hefti F, Melamed E, Wurtman RJ. Partial lesions of the dopaminergic nigrostriatal system in rat brain: biochemical characterization. *Brain Res.* 1980;195:123–137.
143. McCaman RE, McCaman MW, Hunt JM, et al. Microdetermination of monamine oxidase and 5HTP decarboxylase activity in nervous tissue. *J Neurochem.* 1965;12:15–23.
144. Cumming P, Gjedde A. Compartmental analysis of dopa decarboxylation in living brain from dynamic positron emission tomograms. *Synapse.* 1998;29:37–61.
145. Arai R, Karasawa N, Geffard M, et al. Immunohistochemical evidence that central serotonin neurons produce dopamine from exogenous L-DOPA in the rat, with reference to the involvement of aromatic L-amino acid decarboxylase. *Brain Res.* 1994;667:295–299.
146. Mura A, Jackson D, Manley MS, et al. Aromatic L-amino acid decarboxylase immunoreactive cells in the rat striatum: a possible site for the conversion of exogenous L-DOPA to dopamine. *Brain Res.* 1995;704:51–60.
147. Melamed E, Hefti F, Pettibone DJ, et al. Aromatic L-amino acid decarboxylase in rat corpus striatum: implications for action of L-dopa in parkinsonism. *Neurology.* 1981;31:651–655.
148. Bowsher RR, Henry DP. In: Bowlton AA, Baker JB, and Yu PH, eds. *Neuromethods. Series 1: Neurochemistry, Neurotransmitter Enzymes.* Clifton, NJ: Humana Press; 1986;33–77.
149. Neff NH, Hadjiconstantinou M. Aromatic L-amino acid decarboxylase modulation and Parkinson's disease. *Prog Brain Res.* 1995;106:91–97.
150. Doteuchi M, Wang C, Costa E. Compartmentation of dopamine in rat striatum. *Mol Pharmacol.* 1974;10:225–234.
151. Groppetti A, Algeri S, Cattabeni F, et al. Changes in specific activity of dopamine metabolites as evidence of a multiple compartmentation of dopamine in striatal neurons. *J Neurochem.* 1977;28:193–197.
152. Farde L. The advantage of using positron emission tomography in drug research. *Trends Neuroscience.* 1996;19:211–214.
153. Burns HD, Hamill TG, Eng W, et al. Positron emission tomography neuroreceptor imaging as a tool in drug discovery, research and development. *Curr Opin Chem Biol.* 1999;3:388–394.
154. Lipinski CA, Lombardo F, Dominy BW, et al. Experimental and computational approaches to estimate solubility and permeability in drug discovery and development settings. *Adv Drug Deliv Rev.* 1997;23:3–25.
155. McGregor MJ, Muskal SM. Pharmacophore fingerprinting. 1. application to QSAR and focused library design. *J Chem Inform Comp Sci.* 1999;39:569–574.
156. Food and Drug Administration Modernization Act of 1997. Public Law 105–115-Nov. 21, 1997.